

A Unified Framework for Surface Flux-Driven Cyclones Outside the Tropics

Kerry Emanuel, Tommaso Alberti, Stella Bourdin, Suzana Camargo, Davide Faranda, Manos Flaounas, Juanje Gonzalez-Aleman, Chia-Ying Lee, Marcello Miglietta, Claudia Pasquero, Alice Portal, Hamish Ramsay, Romualdo Romero

Abstract

Cyclonic storms resembling tropical cyclones are sometimes observed well outside the tropics. These include medicanes, polar lows, subtropical cyclones, Kona Storms, and possibly some cases of Australian East Coast Cyclones. Their structural similarity to tropical cyclones lies in their tight, nearly axisymmetric inner cores, eyes, and spiral bands. Previous studies of these phenomena suggest that they are partly and sometimes wholly driven by surface enthalpy fluxes, as with tropical cyclones. Here we show, through a series of case studies, that these non-tropical cyclones have morphologies and structures that resemble each other and also closely match those of tropical transitioning cyclones, with the important distinction that the potential intensity that supports them is not present in the pre-storm environment but rather is locally generated in the course of their development. We therefore propose to call these storms CYClones from Locally Originating Potential intensity (CYCLOPs). Like their tropical cousins, the rapid development and strong winds of cyclops pose a significant threat and forecast challenge for islands and coastal regions.

1. Introduction

Cyclones that resemble tropical cyclones are occasionally observed to develop well outside the tropics. These include polar lows, medicanes, subtropical cyclones, Kona Storms (central North Pacific), and perhaps some cases of Australian East Coast Cyclones. The identification of such systems is usually based on their appearance in satellite imagery and on the environmental conditions in which they occur. Here we show that many of these systems are manifestations of the same physical phenomenon and, as such, should be given a common, physically-based designation. We propose to call these CYClones from Locally Originating Potential intensity (CYCLOPs), with reference to the single-eyed creatures of Greek mythology. We show that in many respects these developments resemble classical “tropical transition” (TT) events, but they are distinguished from the latter by occurring in regions where the climatological potential intensity is small or zero. The short development time scale and intense mesoscale inner cores make cyclops significant hazards and a forecasting challenge.

Cyclones of synoptic and sub-synoptic scale are powered by one or both of two energy sources: the available potential energy (APE) associated with isobaric temperature gradients (baroclinity), and fluxes of enthalpy (sensible and latent heat) from the ocean to the

atmosphere¹. A normal extratropical cyclone over land is an example of the former, while the latter is epitomized by a classical tropical cyclone. Extratropical transitioning, tropical transitioning, and hybrid cyclones are powered by both sources, with the relative proportion usually varying over the life of the storm. We note that tropical cyclones often originate in disturbances, such as African easterly waves, that derive their energy from isobaric temperature gradients.

Like tropical cyclones, cyclops are powered by surface enthalpy fluxes, but differ from the former in that the required potential intensity is produced locally and transiently by baroclinic processes, whereas it is always present in the seasons and regions where tropical cyclones develop. Cyclops closely resemble the strongly baroclinic cases of tropical transition defined and discussed by Davis and Bosart (2004), except that they occur in regions where the climatological potential intensity is too small for tropical cyclogenesis, relying on synoptic-scale perturbations that locally enhance potential intensity in space and time. (Bosart and Davis (2004) confined their attention to tropical cyclone formation in regions of high sea surface temperature, stating that ““The precursor cyclone must occlude and remain over warm water (>~26°C) for at least a day following occlusion.” Similarly, McTaggart-Cowan et al. (2008) and McTaggart-Cowan et al. (2013) only examined cases of tropical transition that resulted in named tropical cyclones.)

The basic physics of cyclops were explored by the first author (Emanuel 2005) in reference to medicanes, and is illustrated in Figure 1. While the actual evolution is, of course, continuous, it is simpler to discuss it in phases. In the first phase (Figure 1a), Rossby wave breaking has resulted in isolated potential vorticity (PV) anomaly near the tropopause. We idealize this anomaly as circularly symmetric and show a cross-section through it. To keep the illustration as simple as possible, the first phase is assumed to occur over land, but that need not be the case in general.

¹ Some would regard latent heating as an additional energy source, but condensation through a deep layer is present in most cyclones and, being strongly tied to vertical motion, should not be regarded as an external heat source but rather as a modification of the effective static stability.

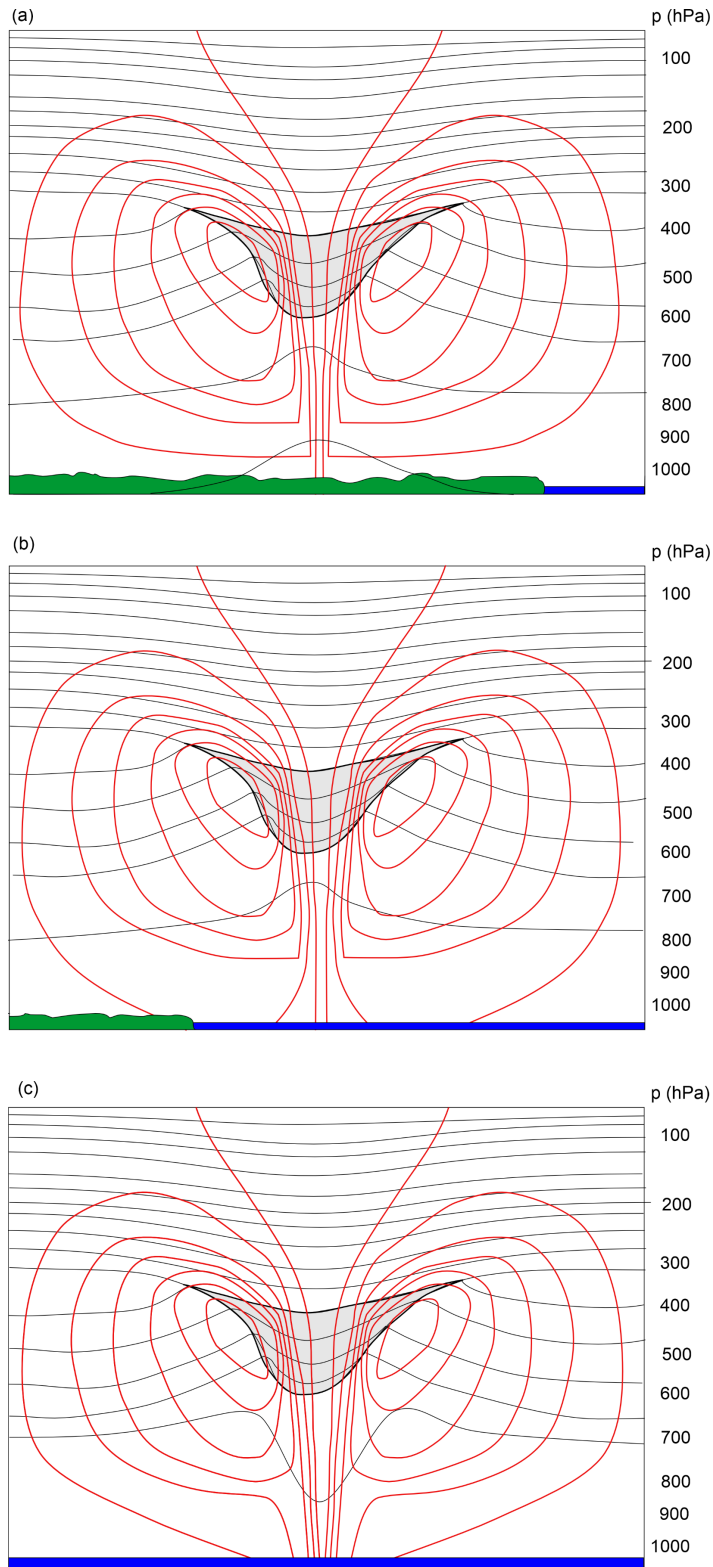


Figure 1: Three stages in the development of a cyclone. Each of the three panels shows a cross-section through a circular, isolated PV anomaly at the tropopause (gray shading). The thick black curves are isentropes, while the red curves are isotachs of the flow normal to the cross-section. In the first phase (a), the PV anomaly is over land, the troposphere beneath it is anomalously cold, and there is no flow at the surface. The system moves out over open water in the next phase (b) and warming of the boundary layer and lower troposphere suffices to eliminate the cold anomaly at and near the surface. Weak cyclonic flow develops in response to the positive PV anomaly aloft. In the final phase (c), the WISHE mechanism comes to life and a tight, inner warm core develops.

During the creation of the near-tropopause PV anomaly, some combination of lifting and cold air seclusion has cooled and moistened the column underneath the PV anomaly, and the cold anomaly extends right to the surface. From a PV inversion perspective, the near-surface anticyclone that results from inverting the negative potential temperature anomaly at the surface is assumed to just cancel the cyclonic anomaly that results from inverting the tropopause PV anomaly, yielding no circulation at the surface.

In phase 2 (Figure 1b), the system drifts out over open water that is warm enough to diminish and eventually eliminate the cold anomaly at the surface, “unshielding” it from the PV anomaly aloft. During this phase, a cyclonic circulation develops in the lower troposphere, with a horizontal scale commensurate with that of the PV anomaly.

If the local potential intensity is large enough, and the air aloft sufficiently close to saturation, Wind-Induced Surface Heat Exchange (WISHE) can develop a tropical cyclone-like vortex (phase 3, Figure 1c), with a warm inner core, eye and eyewall, and perhaps spiral bands. Note that the inner core may be warm only with the respect to the synoptic-scale cold anomaly surrounding it, not necessarily with respect to the distant environment. At mid-levels, the temperature anomaly may manifest as a small-scale warm anomaly surrounded by a synoptic-scale cold anomaly.

In reality, these phases blend together into a continuum. One practical challenge is calculating the potential intensity. This should be calculated under the PV anomaly aloft but before the troposphere has appreciably warmed from surface fluxes. However, in practice, the warming occurs as the PV anomaly develops over water, or as it moves out over water from land. The true potential intensity for a TC developing within the cold column under the PV anomaly should be calculated using the sea surface temperature and the sounding of the free troposphere *before* it has warmed up. In practice, we do not have access to such a hypothetical sounding. Nevertheless, we can estimate how cold the troposphere was before surface fluxes warmed it by assuming that the troposphere has an approximately moist adiabatic temperature profile and using the upper tropospheric geopotential height in the cold cutoff cyclone to estimate the negative temperature perturbation underneath it. This was done in Emanuel (2005) and a slightly improved version derived in the Appendix. The result is a modified potential intensity, V_{pm} , given by

$$V_{pm}^2 = V_p^2 - \frac{C_k}{C_D} \frac{T_s}{T_{400}} \phi'_{400}, \quad (1)$$

where V_p is the potential intensity calculated in the usual way from the local sea surface temperature and atmospheric sounding, ϕ'_{400} is the perturbation of the upper tropospheric geopotential, which we here evaluate at 400 hPa, away from climatology, C_k and C_D are the surface exchange coefficients for enthalpy and drag, and T_s and T_{400} are the absolute temperatures at the surface and 400 hPa. In what follows, we approximate the coefficient multiplying ϕ'_{400} in (1) by a constant value, 1.3.

Beginning with an upper cold cyclone in an environment of otherwise zero potential intensity, Emanuel (2005) simulated the development of a WISHE-driven cyclone using the axisymmetric, nonhydrostatic hurricane model of Rotunno and Emanuel (1987). The cold, moist troposphere under such an upper cyclone proves to be an ideal incubator of surface flux-driven cyclones with characteristics nearly identical to those of tropical cyclones. One interesting facet of the process is that the anomalous surface enthalpy flux destroys the parent upper cold low over a period of a few days.

2. Why it matters

Why should we care whether a cyclone is driven by surface fluxes or baroclinity? From a practical forecasting standpoint, the distributions of weather hazards, like rain and wind, can be very different, as can be the development time scales and fundamental predictability.

In classical baroclinic cyclones, the strongest winds are often found in frontal zones and can be far from the cyclone center, and precipitation is usually heaviest in these frontal zones and in a shield of slantwise ascent extending poleward from the surface cyclone. There is long experience in forecasting baroclinic storms, and today's numerical weather prediction (NWP) of these events has become quite accurate, even many days ahead. Importantly, baroclinic cyclones are well resolved by today's NWP models. While baroclinic cyclones can intensify rapidly, both the magnitude and timing of intensification are usually forecast accurately, and uncertainties are well quantified by NWP ensembles.

By contrast, the physics of tropical cyclone intensification, involving a positive feedback between surface winds and surface enthalpy fluxes, results in an intense, concentrated core with high winds and heavy precipitation (which can be snow in the case of polar lows). The eyewalls of surface flux-driven cyclones are strongly frontogenetical, further concentrating wind and rain in an annulus of mesoscale dimensions. The intensity of surface flux-driven cyclones can change very rapidly and often unpredictably, presenting a severe challenge to forecasters. For example, Hurricane Otis of 2023 intensified from a tropical storm to a Cat 5 hurricane in about 30 hours, devastating Acapulco, Mexico, with little warning from forecasters. The small size of the core of high winds and heavy precipitation means that small errors in the forecast position of the storm lead to large errors in local wind and precipitation. Surface flux-driven cyclones are too small to be well resolved by today's global NWP models, and even if they were, fundamental predictability studies show high levels of intrinsic unpredictability of rapid intensity changes (Zhang et al. 2014).

The time and space scales of surface flux-driven cyclones are such that they couple strongly with the ocean, producing near-inertial currents whose shear-driven turbulence mixes to the surface generally (but not always) colder water from below the surface mixed layer. This has an important (usually negative) feedback on the intensification of such cyclones. Accurate numerical forecasting of surface flux-driven cyclones therefore requires an interactive ocean, generally missing from today's NWP models because it is not very important for baroclinic cyclones and because of the additional computational burden.

For these reasons, it matters (or should matter) to forecasters whether a particular development is primarily driven by surface fluxes or by ambient baroclinity. The structural differences described above are often, but not always, detectable in satellite imagery; at the same time, such imagery is sometimes misleading about the underlying physics. For example, classical baroclinic development sometimes develops cloud-free eyes surrounded by convection, through the warm seclusion process, even over land, and yet may not have the intense annular concentration of wind and rain characteristic of surface flux-driven cyclones (Tous and Romero 2013).

Armed with the conceptual cyclop model developed in section 1 and modified potential intensity given by (1), we now turn to case studies of the development of medicanes, polar lows, a subtropical cyclone, and a Kona Storm, showing that the dynamic and thermodynamic pathways are similar. Specifically, each case developed after the formation of a deep, cold-core cut-off cyclone in the upper troposphere that often resulted from a Rossby wave breaking event. The lifting of the tropospheric air in response to the developing potential vorticity anomaly near the tropopause created a deep, cold, and presumably humid column. The deep cold air over bodies of water substantially elevates potential intensity, while its high relative humidity discourages evaporatively driven convective downdrafts, which tamp down the needed increase in boundary layer enthalpy. Low shear near the core of the cutoff cyclone, coupled with high potential intensity and humidity, provide an ideal embryo for tropical cyclone development.

In what follows we focus on the cutoff cyclone evolution and the development of modified potential intensity. In a particular case, we compare reanalysis column water vapor to that estimated from satellite measurements. The differences between these are significant enough to cast some doubt on the quality of reanalyzed water vapor associated with the small-scale cyclop developments, thus we do not focus on water vapor even though it is known to be important for intensification of tropical cyclones.

We also examined, but do not show here, several cases of Australian east coast cyclones. Owing to the east Australian Current, the climatological potential intensity is substantial off the southeast coast of Australia, and the developments we analyzed behaved more like classical tropical transitions, with little or no role of the synoptic scale dynamics in enhancing the existing potential intensity. We suspect that there may be other cases in which the latter process was important, but did not conduct a search for such cases.

Yet, as is the case with tropical cyclones, there are variations on the theme, and we explore these in the closing sections.

3. Case Studies

a. Medicanes of January, 1995

On average, 1.5 medicanes are observed annually in the Mediterranean (Cavicchia et al. 2014; Romero and Emanuel 2013; Nastos et al. 2018; Zhang et al. 2021) and, more rarely, similar

storms are observed over the Black Sea (Yarovaya et al. 2008) . We begin with a system, Medicane Celeno, that reached maturity on 16 January, 1995, shown in infrared satellite imagery in Figure 2.

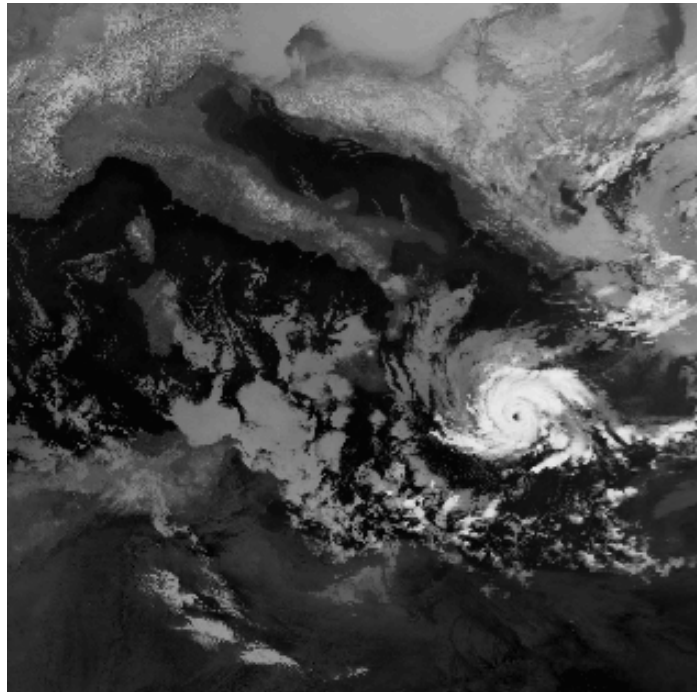


Figure 2: Infrared satellite image of Medicane Celeno in the central Mediterranean, at 09:06 UTC 16 January 1995.

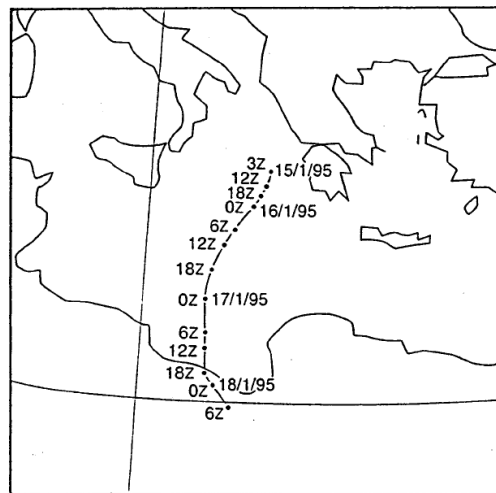


Figure 3: Track of the surface center of the cyclone between 03:00 UTC on January 15 and 06:00 on January 18, 1995, derived from satellite images.

Figure 3 shows the track of the surface center of the cyclone, which developed between Greece and Sicily and made landfall in Libya. A detailed description of this medicane is provided by Pytharoulis et al. (1999).

The evolution of the system in increments of 24 hours, beginning on 00 GMT, 12 January and ending at 00 GMT 15 January, is shown in Figure 4. This sequence covers the period just before the system develops and shows the 400 hPa and 950 hPa geopotential heights. The evolution of the upper tropospheric (400 hPa) height field shows a classic Rossby wave breaking event (McIntyre and Palmer 1983) in which an eastward-moving baroclinic Rossby wave at higher latitudes amplifies and irreversibly breaks to the south and west, finally forming a cut-off cyclone. To the southeast of this trough. A weak, broad area of low pressure develops mostly over land in a region of low-level warm advection. As the cold pool is gradually heated by the underlying sea, a broad surface cyclone develops by 00 GMT on January 14th. At around this time, the feedback between surface wind and surface enthalpy fluxes is strong enough to develop a tight inner warm core (warm, that is, relative to the surrounding cold pool, not necessarily to the unperturbed larger scale environment) by 00 GMT on January 15th, noticeable just to the west of northwestern Greece (Figure 5d; see inset). At the same time, the upper cold core weakens, no doubt aided by the strong heating from the surface transferred aloft by deep convection.

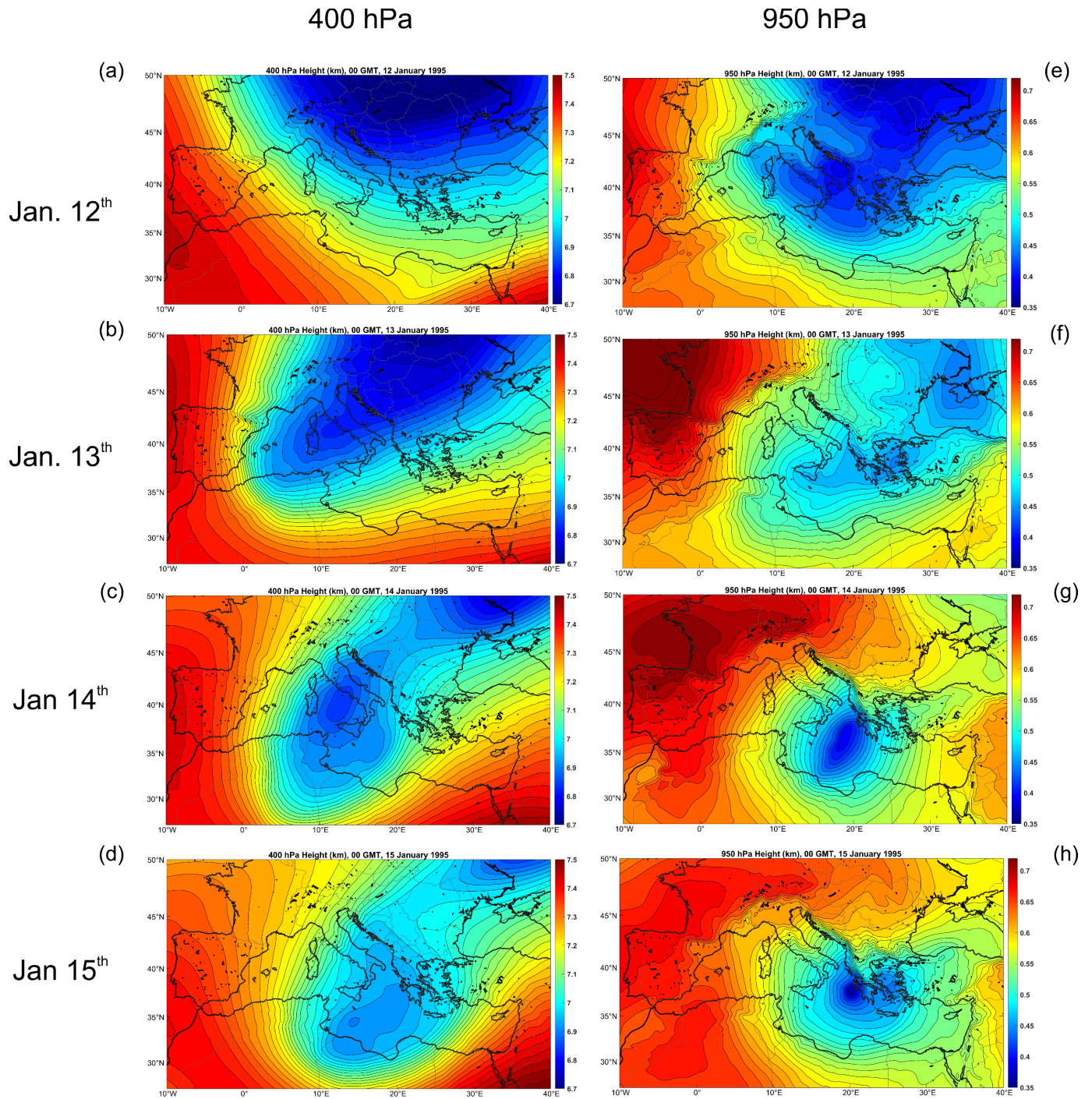


Figure 4: Evolution of the 400 hPa (left) and 950 hPa (right) geopotential heights in 24-hour increments, from 00 GMT 12 January to 00 GMT 15 January, 1995. These fields are from ERA5 reanalyses. The 400 hPa heights span from 6.7 to 7.5 km, while the 950 hPa heights range from 350 m to 730 m.

750 hPa T (K)

Modified Potential Intensity (m/s)

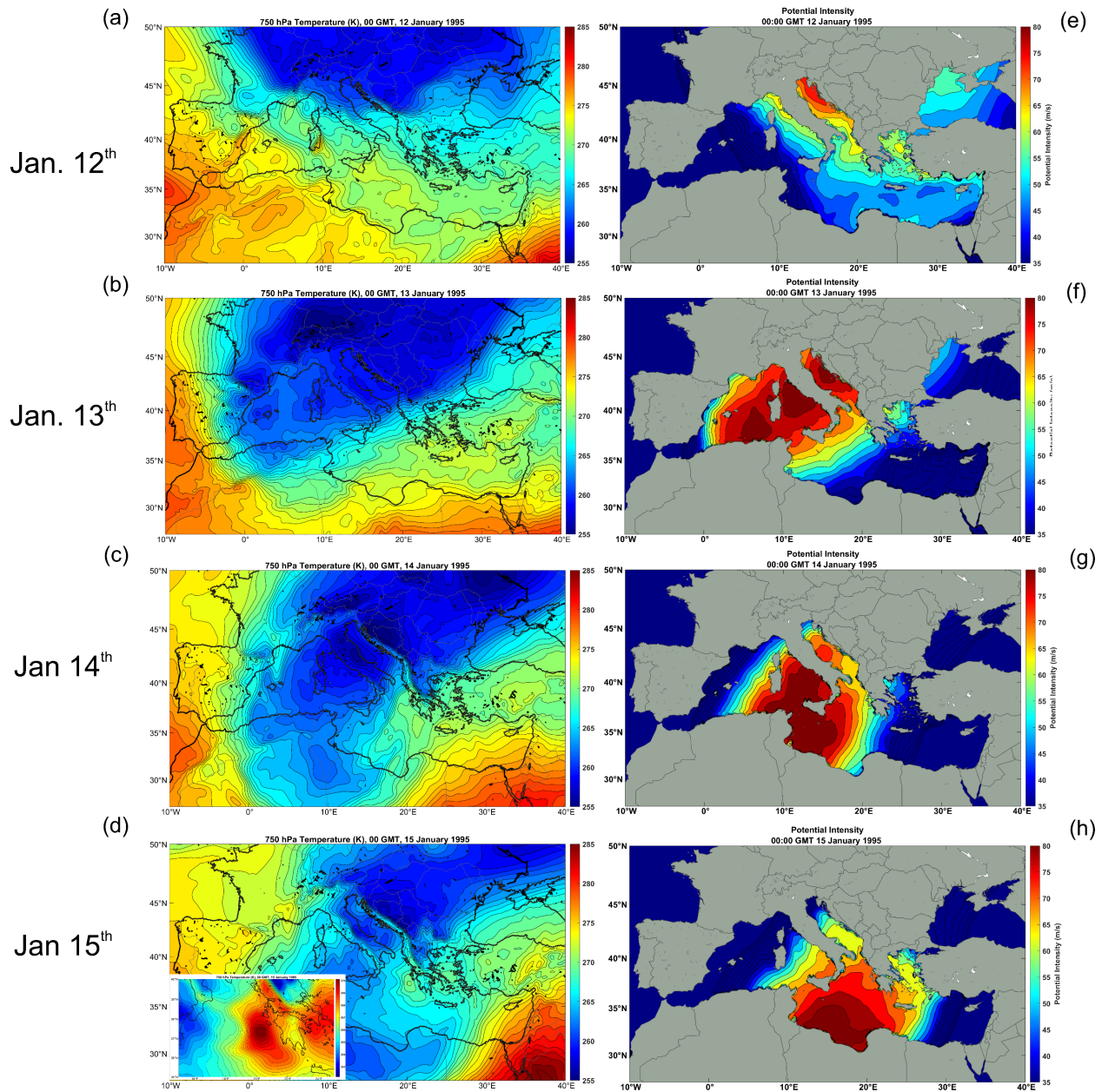


Figure 5: 750 hPa temperature (K; left) and modified potential intensity given by (1) (m/s, right) at 00 GMT on January 12th – 15th (top to bottom) 1995. The inset in (d) zooms in on the cyclop just west of the Peloponnese. The 850 hPa temperature spans from 255 K to 285 K, while the modified potential intensity ranges from 35 to 80 ms⁻¹. From ERA5 reanalyses.

Figure 5 shows the corresponding evolution of the 750 temperature and the modified potential intensity, V_{pm} , given by (1). The latter in this and subsequent figures is only shown in the range of 35 m s^{-1} to 80 m s^{-1} . Experience shows that tropical cyclone genesis is rare when the potential intensity is less than about 35 m s^{-1} (Emanuel 2010).

On January 12th, relatively small values of V_{pm} are evident in the eastern and northern Mediterranean, but with higher values developing over the northern Adriatic as cold air aloft creeps in from the north. As the upper tropospheric Rossby wave breaks and a cut-off cyclone develops over the central Mediterranean, V_{pm} increase greatly during the 13th and 14th, with peak values greater than 80 m s^{-1} . The cyclop develops in a region of very high V_{pm} , though not where the highest values occur. Note that a lower warm core is not obvious at 750 hPa until January 15th and that it occurs on a somewhat smaller scale than the cut-off cyclone.

As the cyclop moves southward, it maintains a tight inner warm core until after landfall (not shown here) and the modified potential intensity, V_{pm} , over the south central Mediterranean diminishes rapidly, with peak values of only about 60 m s^{-1} by 00 GMT on January 17th. One potentially important difference between cyclop development and tropical transition is that in the former case, the volume of air with appreciable potential intensity is limited, and it is possible that the enhanced surface fluxes associated with the cyclop substantially diminish the magnitude and/or volume of the high V_{pm} air, serving to limit the lifetime of the cyclop. This was the case in the axisymmetric numerical simulations of Emanuel (2005).

It is clear in this case that the cyclop developed on time and space scales appreciably smaller than those of the rather weak, synoptic-scale cyclogenesis resulting from the interaction of the positive PV perturbation near the tropopause with a low-level temperature gradient. It is also clear that the strong cooling of the troposphere in response to the development and southward migration of the cutoff cyclone aloft was instrumental in bringing about the high potential intensity necessary for the WISHE process. Thus the Rossby wave breaking did much more than trigger cyclogenesis; it provided the necessary potential intensity for the development. In this respect, it differs from tropical transition, though in that case, it is possible that the upper trough enhances the existing potential intensity.

b. Medicane of December 2005

A medicane, unofficially known as Zeo, formed on December 14th 2005 off the coast of Tunisia and then moved eastward across a large stretch of the Mediterranean. Figure 6 shows a satellite image of this medicane on December 15th. This cyclone has been the subject of several intensive studies (e.g. Fita and Flaounas 2018; Miglietta et al. 2021).

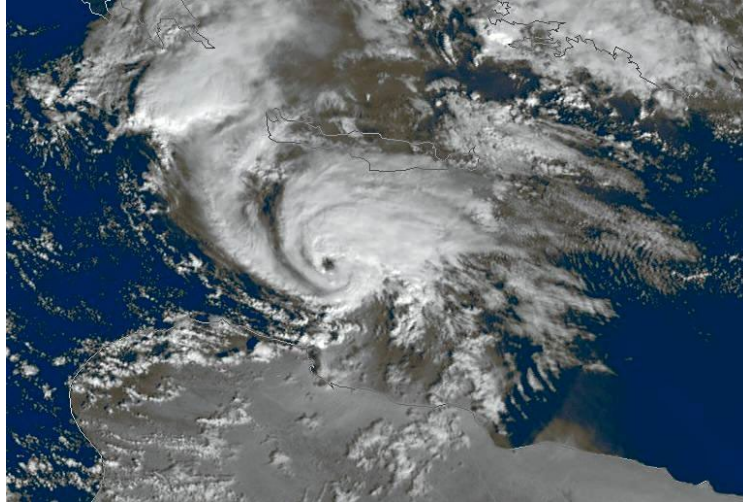


Figure 6: Medicane between Crete and Libya on 15 December 2005.

Like Medicane Celeno, it formed as a result of a Rossby wave breaking event, as illustrated in Figure 7. On December 8th (panel a), a deep trough is digging southward over eastern Europe, but by the 9th (panel b) has split in two, with the westward half breaking southwestward over Germany and Switzerland. By the 11th (panel d), this local minimum is located over Tunisia and on the 12th (panel e) is more or less completely cut off from the main westerly jet. It subsequently oscillates over Tunisia and Algeria, before moving slowly eastward over the Mediterranean, as shown in Figure 8.

In response to the cutoff cyclone development, a broad, synoptic-scale cyclone formed to the east of the upper cyclone over the deserts of Libya during December 12th and 13th (not shown here). The poorly defined center of this system drifted northward, on collision course with the upper cyclone, which was drifting eastward over Tunisia by late on the 13th. As the surface center moved out over the Mediterranean early on the 13th, rapid development ensued and a mature cyclop is evident by 00 GMT on the 14th (Figure 8c). The system began to move eastward and reached peak intensity early on the 15th, though the ERA5 reanalysis has it stronger on the 14th (lower panels of Figure 8). The cyclop moved eastward, along with its parent upper cyclone, and dissipated in the far eastern Mediterranean on the 16th (not shown).

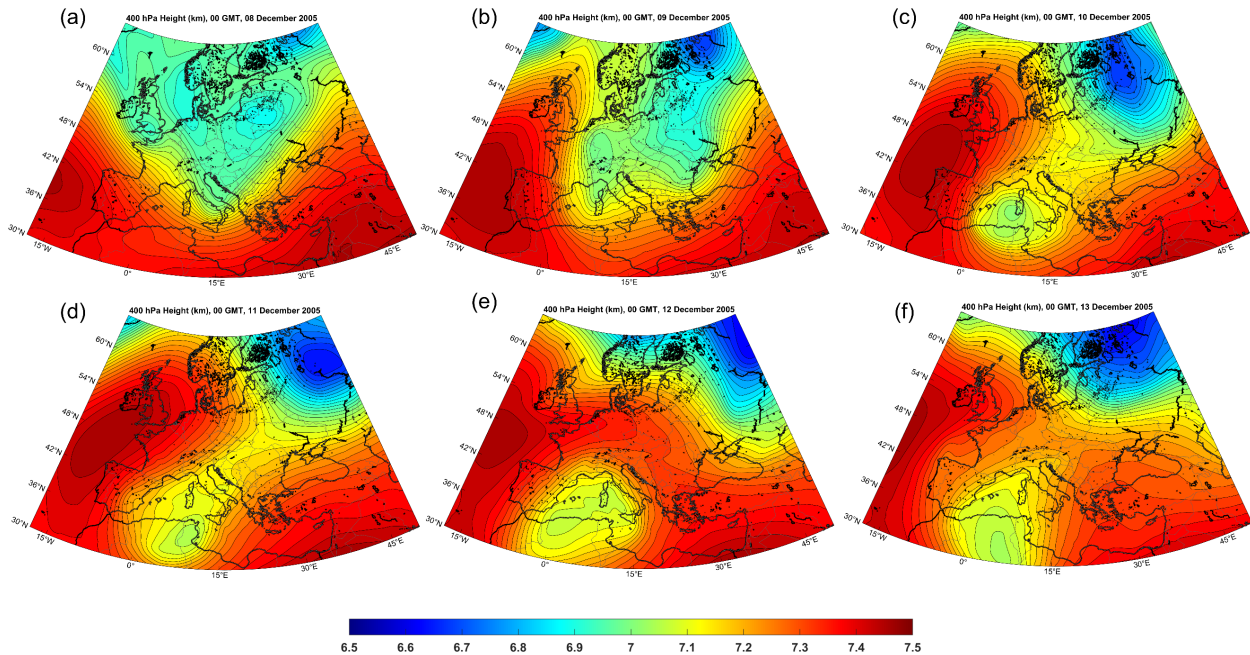


Figure 7: 400 hPa heights, ranging from 6.5 km to 7.5 km (color scale identical for all panels) at 00 GMT on December 8th (a), 9th (b), 10th (c), 11th (d), 12th (e), and 13th (f), 2005. From ERA-5 reanalyses.

The evolutions of 750 hPa temperature and V_{pm} on the 14th and 15th of December are shown in Figure 9. In this case, there were large meridional gradients of sea surface temperature across the Mediterranean, ranging from over 20°C in the far south to less than 12°C in the northern reaches of the Adriatic and western Mediterranean (not shown here). As the cold pool moved southwestward and deepened, only small values of V_{pm} developed over the northern Mediterranean, but beginning on December 10th, larger values develop over the Gulf of Sidra, east of Tunisia and by the 14th (Figure 9c) had reached at least 80 ms⁻¹, enabling the formation of the cyclop. As in the Celano case, V_{pm} diminishes thereafter, possibly because of the surface enthalpy flux.

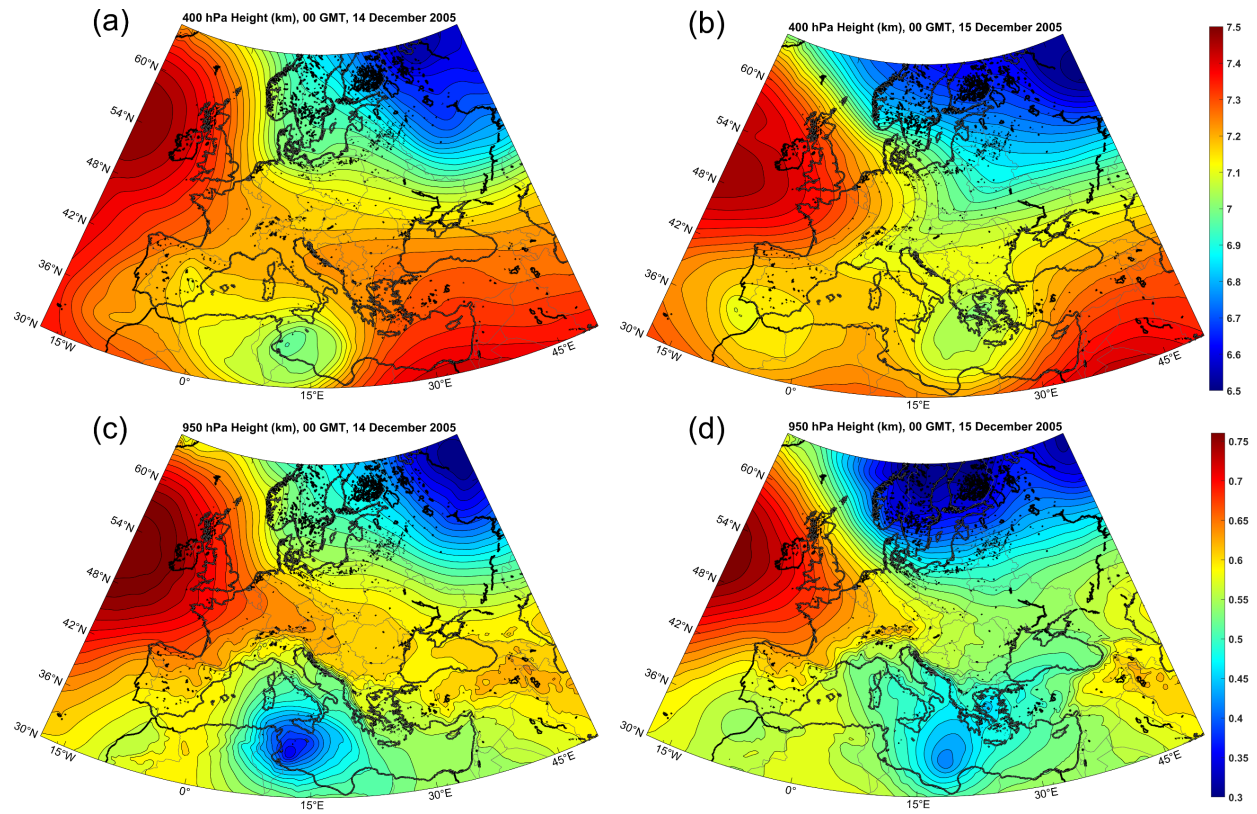


Figure 8: Evolution of 400 hPa height, ranging from 6.5 to 7.5 km (a and b), and 950 hPa height, ranging from 250 to 750 m (c and d) at 00 GMT in December 14th (left) and 15th (right), 2005. The color scales of (a) and (b) are identical, as are the color scales of (c) and (d). From ERA-5 reanalyses.

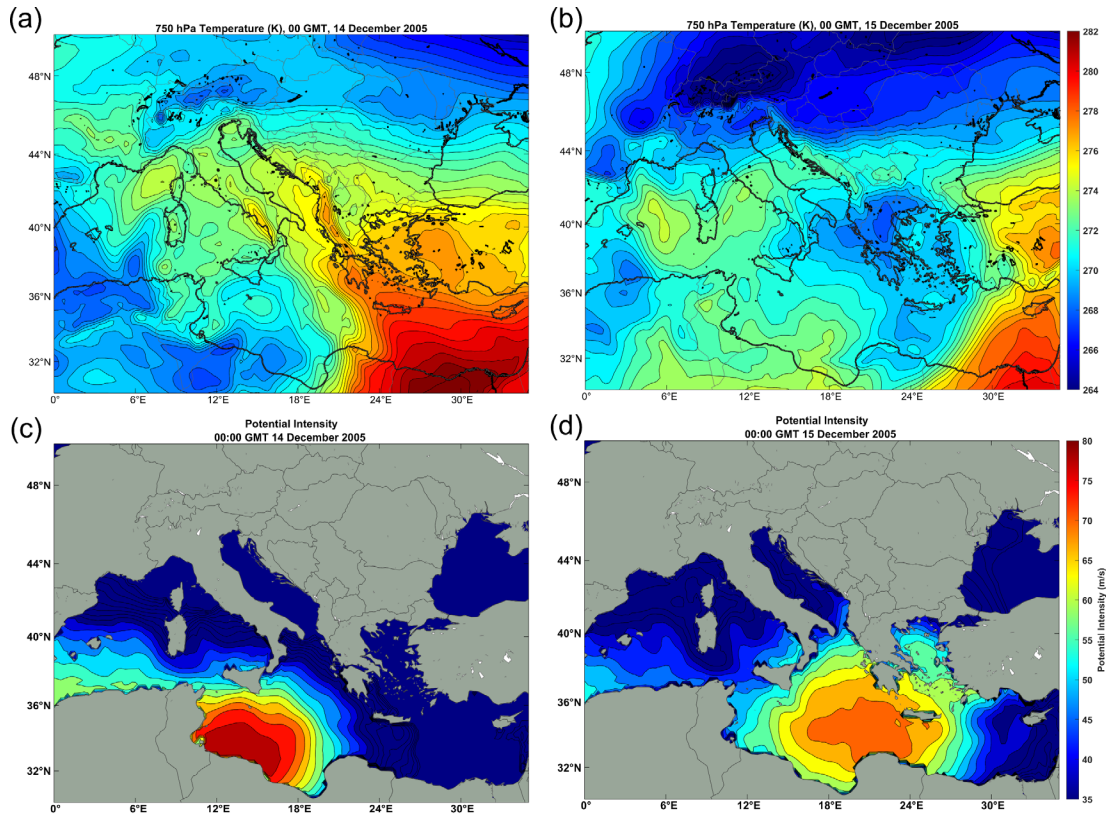


Figure 9: 750 hPa temperature (K; a-b) and modified potential intensity ($m s^{-1}$, c-d) at 00 GMT on December 14th (a,c) and December 15th (b,d) 2005. From ERA-5 reanalyses.

The 750 hPa temperature field (Figure 9a) shows a complex pattern of positive temperature perturbation near the position of the surface low, not nearly as focused as in the case of medicane Celano. As suggested by Fita and Flaounas (2018), some of the temperature anomaly associated with the cyclone may have resulted from warm seclusion. Yet 24 hours later (Figure 9b) the warm anomaly near the cyclone center over the eastern Gulf of Sidra appears to have been advected from the south rather than the north. It is possible that the reanalysis did not capture all of the physics of this particular medicane.

Figure 10 compares total column water retrieved from satellite microwave and near-infrared imagers (a) to that from the ERA5 reanalysis (b). While there is some broad agreement between the two estimates, the ERA5 underestimates column water in the critical region just east of Tunisia and overestimates it in an arc extending from eastern Sicily southeastward to the Libyan coast. Cyclop intensity, in analogy to tropical cyclone intensity, should be highly sensitive to moisture in the mesoscale inner core region, and may be under-resolved and otherwise not well simulated by global NWP models. For this reason, we do not routinely show reanalysis water vapor analyses in this paper.

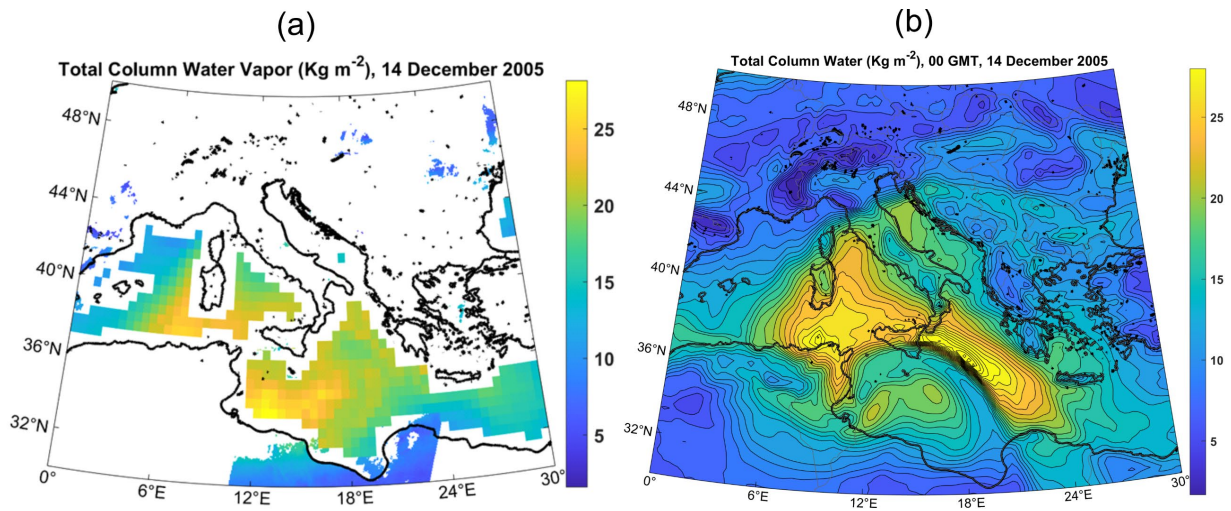


Figure 10: Total column water vapor (Kg m^{-2}) at 00 GMT on 14 December 2005, derived from microwave and near infrared imagers (a) and ERA5 reanalysis (b).

c. Polar low of February, 1987

Closed upper tropospheric lows also provide favorable environments for cyclop developments at very high latitudes in locations where there is open water. These usually form poleward of the mid-latitude jet, where quasi-balanced dynamics can be quite different. Figure 11 is an infrared image of a polar low that formed just south of Svalbard on February 25th, 1987, and tracked southward, making landfall on the north coast of Norway on the 27th. This system was studied extensively by Nordeng and Rasmussen (1992).

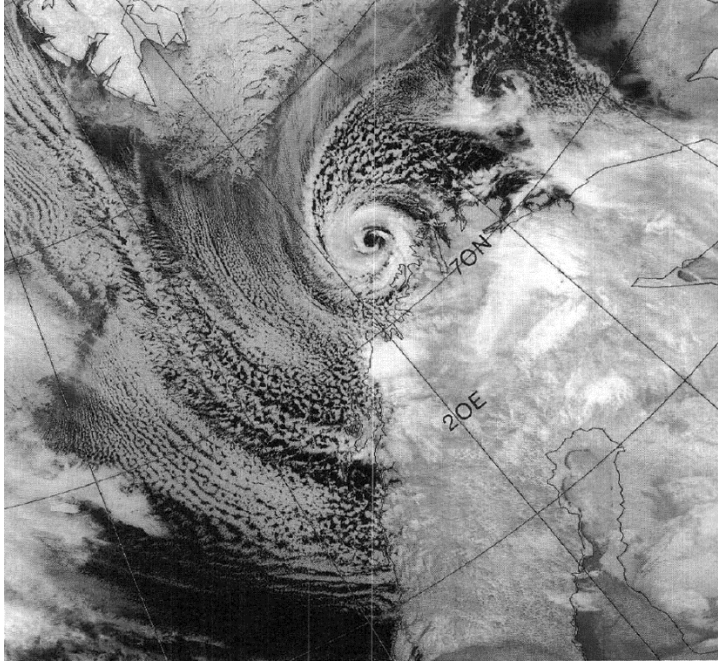


Figure 11: NOAA 9 satellite infrared image (channel 4) of a polar low just north of Norway at 08:31 GMT on 27 February 1987.

As with medicanes, polar lows develop in strongly convecting air masses when cold air moves out over relatively warm water. The adjective “relatively” is crucial here; with polar lows the sea surface temperature is often only marginally above the freezing point of saltwater. Figure 12 shows the distribution of sea surface temperature on February 25th, with the uniform dark blue areas denoting regions of sea ice cover. The polar low shown in Figure 11 develops when deep cold air moves southward over open water, as shown in Figure 13.

In this case, it is not clear whether one can describe what happens in the upper troposphere (top row of Figure 12) as a Rossby wave breaking event. Instead, what we see is a complex rearrangement of the tropospheric winter polar vortex, as a ridge building over North America breaks and forms an anticyclone over the North Pole. This complex rearrangement results in the formation of a deep cutoff low just south of Svalbard by the 26th, which then moves southward over Norway by the 27th. The polar low is barely visible in the 950 hPa height field on the 25th (middle row of Figure 12), but intensifies rapidly as it moves over progressively warmer water, reaching maturity before landfall on the 27th.

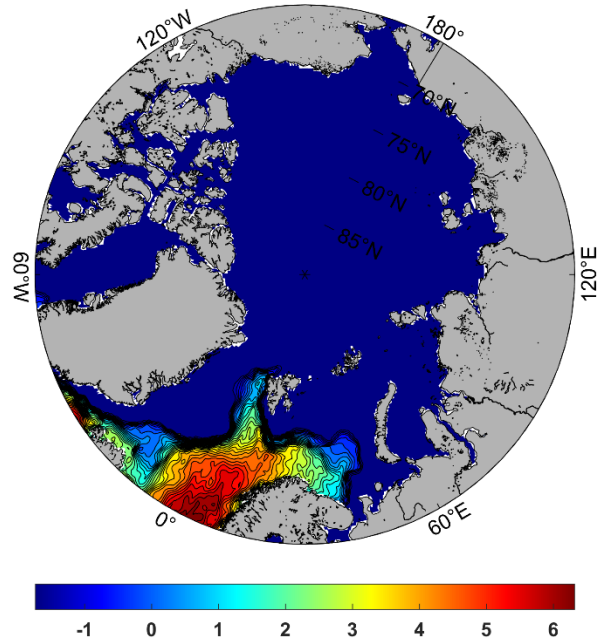


Figure 12: Sea surface temperature (°C) at 02:00 GMT on 25 February, 1987, from ERA5 reanalysis. Dark blue areas denote regions of sea ice. From ERA-5 reanalyses.

The evolution of the V_{pm} field is shown in the bottom row of Figure 13. The potential intensity for cyclops develops rapidly south of Svalbard as the cut-off cyclone moves out over open water.

Under these conditions, almost all the surface flux that drives the cyclop is in the form of sensible, rather than latent, heating, and the background state has a nearly dry (rather than moist) adiabatic lapse rate. As shown by Cronin and Chavas (2019) and Velez-Pardo and Cronin (2023), surface flux-driven cyclones can develop in perfectly dry convecting environments, though they generally reach smaller fractions of their potential intensity and lack the long tail of the radial profile of azimuthal winds that is a consequence of the dry stratification resulting from background moist convection (Chavas and Emanuel 2014). They also have larger eyes relative to their overall diameters. Given the low temperatures at which they occur, polar lows may be as close to the Cronin-Chavas dry limit as one might expect to see in earth's climate.

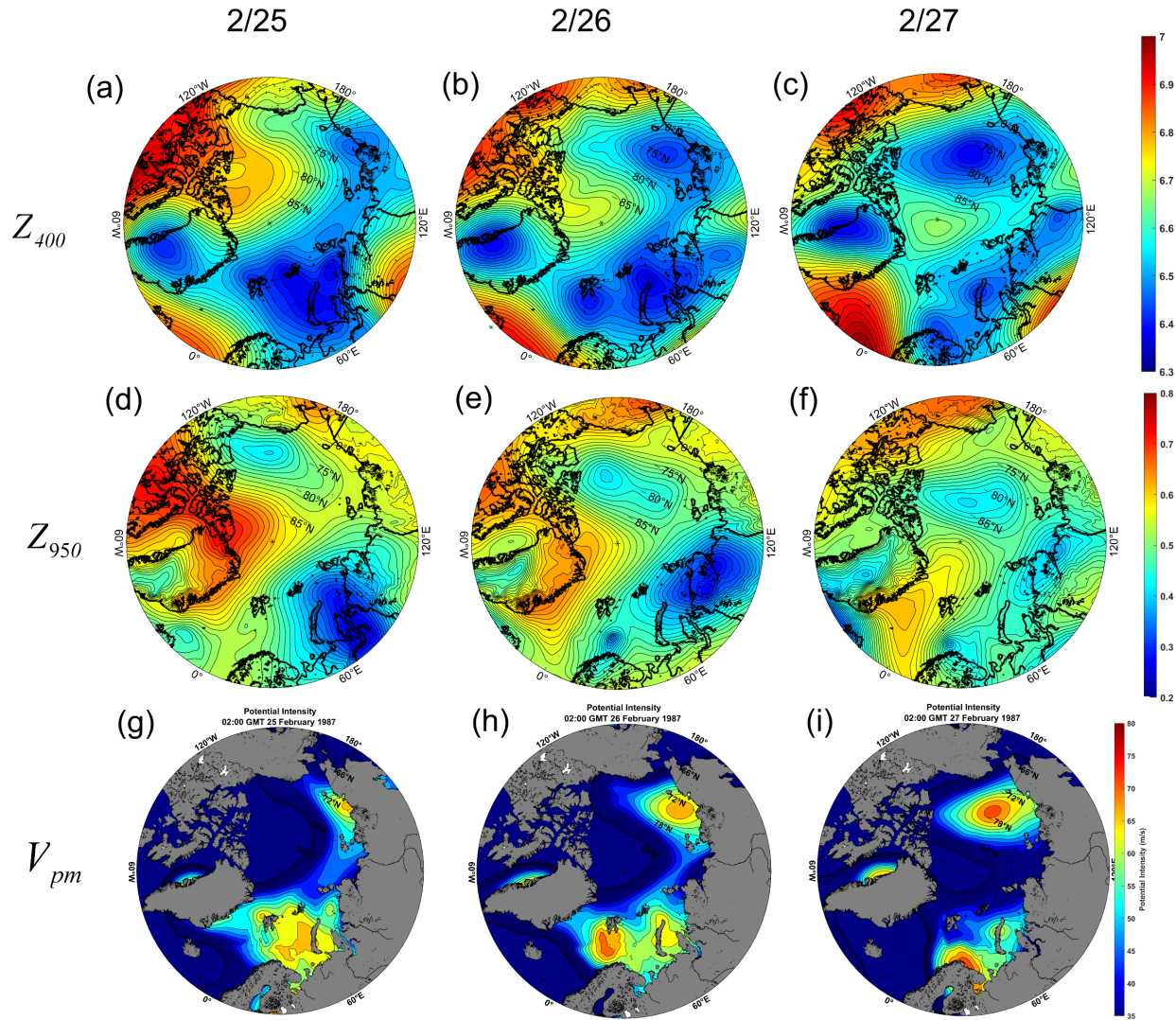


Figure 13: 400 hPa geopotential height (km; a-c), 950 hPa geopotential height (km; dif), and V_{pm} (ms^{-1} , g-i), at 02:00 GMT on February 25th (left), 26th (center), and 27th (right), 1987. From ERA-5 reanalyses.

One interesting feature of polar waters in winter is that the thermal stratification is sometimes reversed from normal, with warmer waters lying beneath cold surface waters. This is made possible, in part, by strong salinity stratification, that keeps the cold water from mixing with the warmer waters below. Therefore, it is possible for polar lows to generate warm, rather than cold, wakes, and this would feed back positively on their intensity. This seems to happen in roughly half the documented cases of polar lows in the Nordic seas (Tomita and Tanaka 2024).

d. Polar low over the Sea of Japan, December, 2009

Polar lows are not uncommon in the Sea of Japan, forming when deep, cold air masses from Eurasia flow out over relatively warm ocean. They are frequent enough to warrant a climatology (Yanase and co-authors 2016). A satellite image of one such storm is shown in Figure 14.

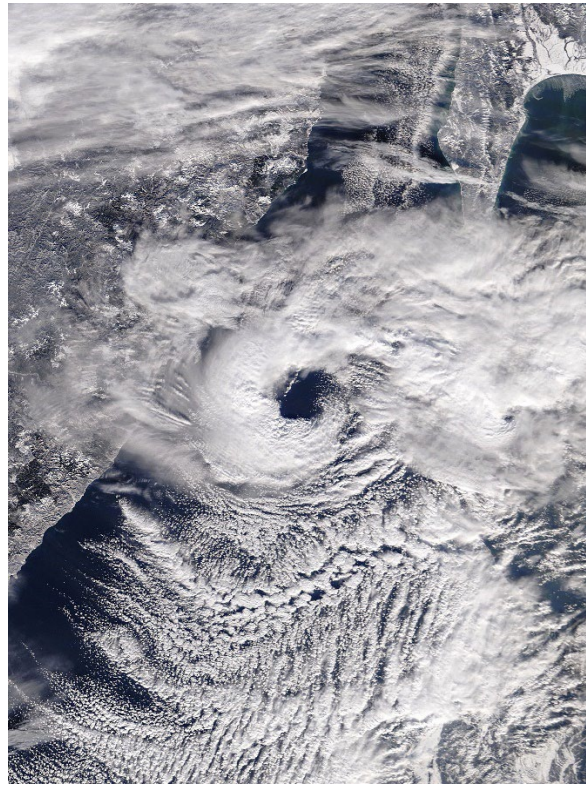


Figure 14: Polar low over the northern Sea of Japan, 02:13 GMT 20 December, 2009 as captured by the MODIS imager on NASA's Terra satellite.

The cyclone traveled almost due south from this point, striking the Hokkaido region of Japan, near Sapporo, with gale-force winds and heavy snow. As with other cyclops, it formed in an environment of deep convection under a cold low aloft.

The development of the cutoff cyclone aloft was complex, as shown by the sequence of 400 hPa maps displayed in Figure 15. These are 00 GMT charts at 1-day intervals beginning on December 11th and ending on the 20th, about the time of the image in Figure 14. A large polar vortex is centered in northern central Russia on the 11th but sheds a child low southeastward on the 12th and 13th, becoming almost completely cutoff on the 14th. The parent low drifts westward during this time. The newly formed cutoff cyclone meanders around in isolation from the 15th through the 17th, but becomes wrapped up with a system propagating in to the domain from the east on the 18th. By the 20th, a small-scale cutoff cyclone is drifting southward over the northern Sea of Japan, and it is this upper cutoff that spawns the polar low.

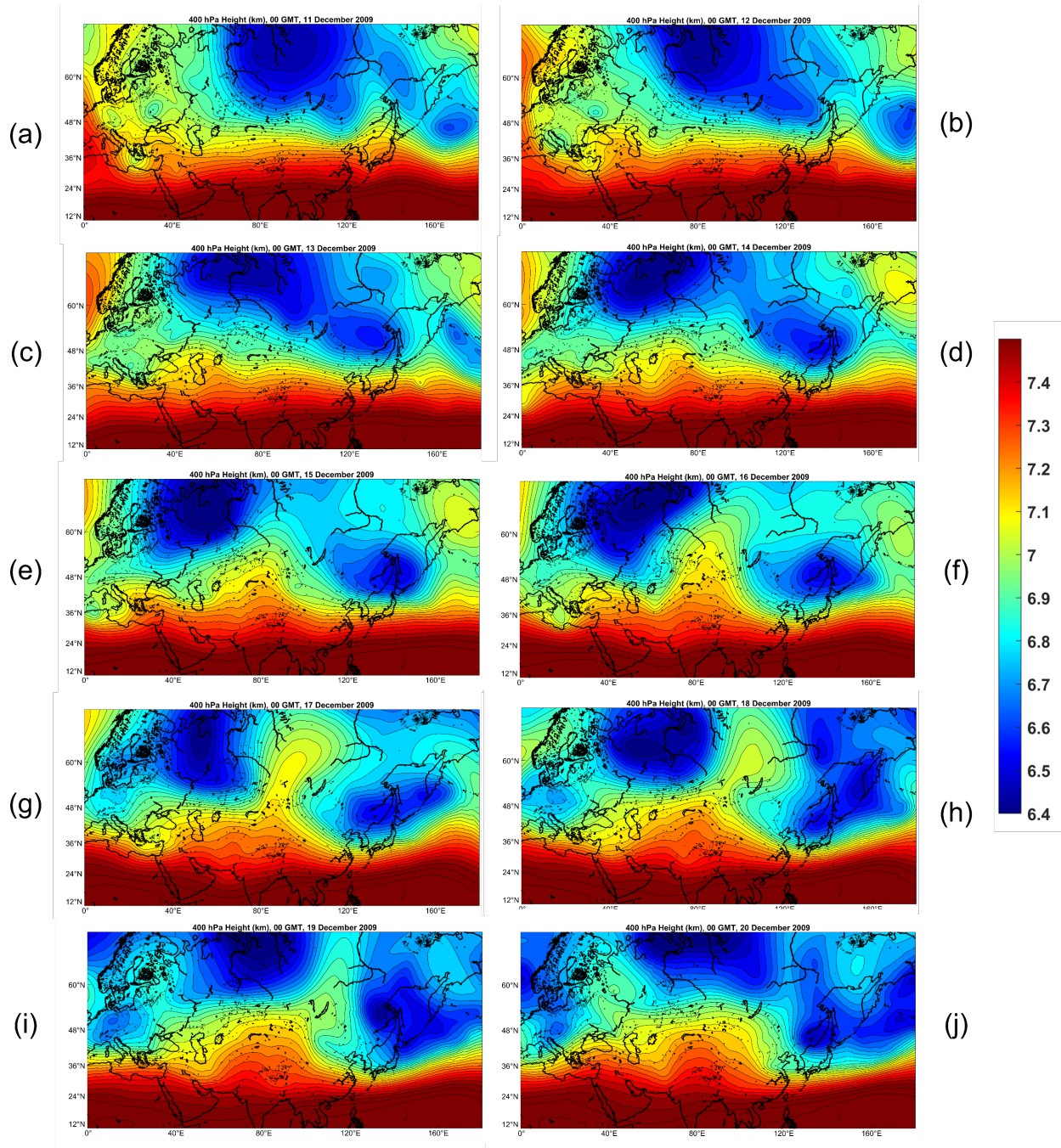


Figure 15: Sequence of 400 hPa geopotential height (km) charts at 1-day intervals from 00 GMT on December 11th (a) to 00 GMT on December 20th (j). The charts span from 0° to 180° longitude and from 10° to 70° latitude. From ERA-5 reanalyses.

The 950 hPa height field and the V_{pm} field at 00 GMT on December 20th are shown in Figure 15.. At this time, the surface low is developing rapidly and moving southward into a region of high potential intensity. The latter reaches a maximum near the northwest coast of Japan, where the sea surface temperatures are larger. As with the two medicane cases and the other polar low case, the cyclop develops in a place where there is normally no potential intensity for surface flux-driven cyclones but for which the required potential intensity is created by the approach of a deep cold cyclone aloft. The reanalysis 750 hPa temperature (not shown) does have a local maximum at the location of the surface cyclone at this time.

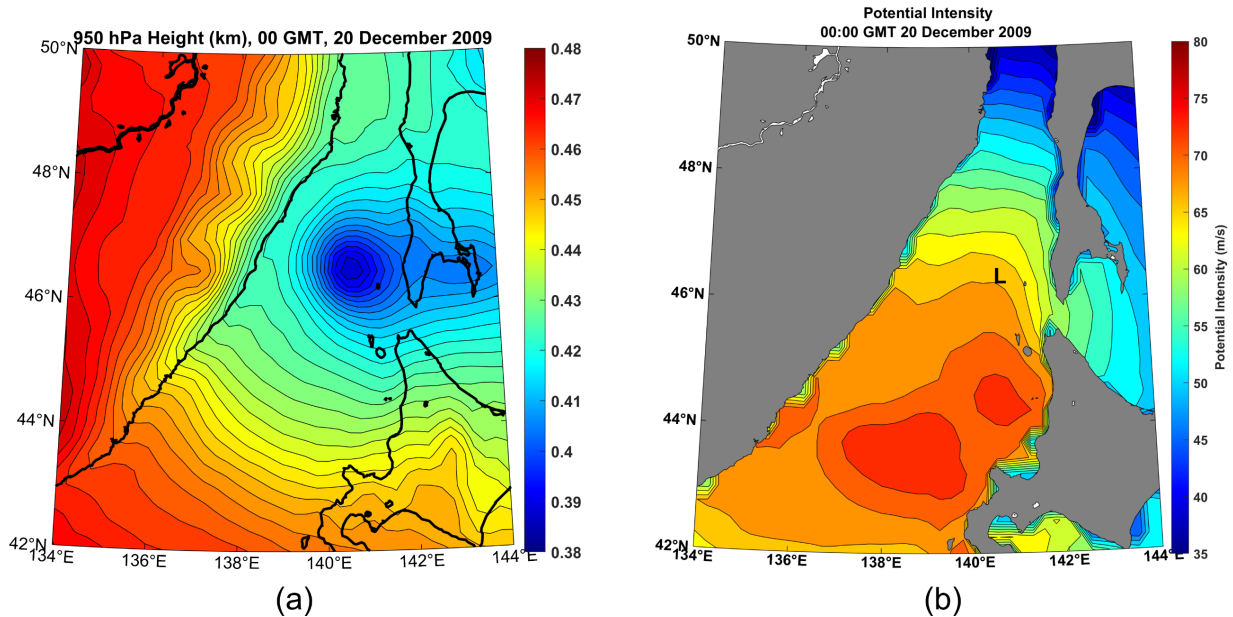


Figure 16: 950 hPa geopotential height (a; km) and V_{pm} (b) at 00 GMT on 20 December, 2009. In (b), the “L” marks the satellite-derived surface cyclone center. From ERA-5 reanalyses.

e. The subtropical cyclone of January, 2023

The term “subtropical cyclone” has been used to describe a variety of surface flux-assisted cyclonic storms that do not cleanly meet the definition of a tropical cyclone. The term has a definite definition in the North Atlantic but is used occasionally elsewhere, especially in regions where terms like medicane, polar low, and Kona storm do not apply. Here we will use the term to designate cyclops in the sub-arctic North Atlantic; that is, surface flux-powered cyclones that develop in regions and times whose climatological thermodynamic potential is small or zero, that would not be called polar lows owing to their latitude. This usage may not be consistent with other definitions. The point here is to show that cyclops can occur in the North Atlantic and we can safely refer to these as cyclops whether or not they meet some definition of “subtropical cyclone”.

Figure 17 displays a visible satellite image of a subtropical cyclone over the western North Atlantic on 16 January, 2023. It resembles the medicanes and polar lows described previously, and like them, formed under a cutoff cyclone aloft.

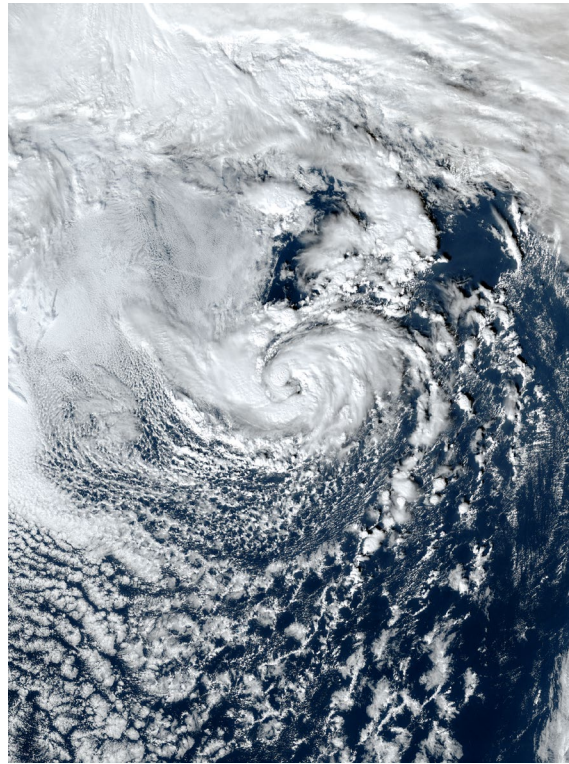


Figure 17: Subtropical cyclone over the western North Atlantic, 18:20 GMT, 16 January 2023.

The formation of the cutoff cyclone aloft is shown in Figure 18. A deep trough advances slowly eastward over eastern North America and partially cuts off on the 14th. As the associated cold pool and region of light shear migrate out over the warm waters south of the Gulf Stream, an cyclop forms and intensifies with peak winds of around 60 kts at around 00 GMT on the 17th (Cangliosi et al. 2023). Note also the anticyclonic wave breaking event to the east of the surface cyclone development.

The evolutions of the 950 hPa field and associated V_{pm} field are displayed in Figure 19. (Note that this figures zooms in to the developing surface cyclone, compared to Figure 18.) On January 14th, the only appreciably large values of V_{pm} are in the Gulf Stream and in the far southwestern portion of the domain. The 950 hPa height field shows a broad trough associated with the baroclinic wave moving slowly eastward off the U.S. east coast. But as the upper cold cyclone moves out over warmer water on the 15th, large V_{pm} develops south of the Gulf Stream, and a closed and more intense surface cyclone develops under the lowest 400 hPa heights and over the region of substantial V_{pm} .

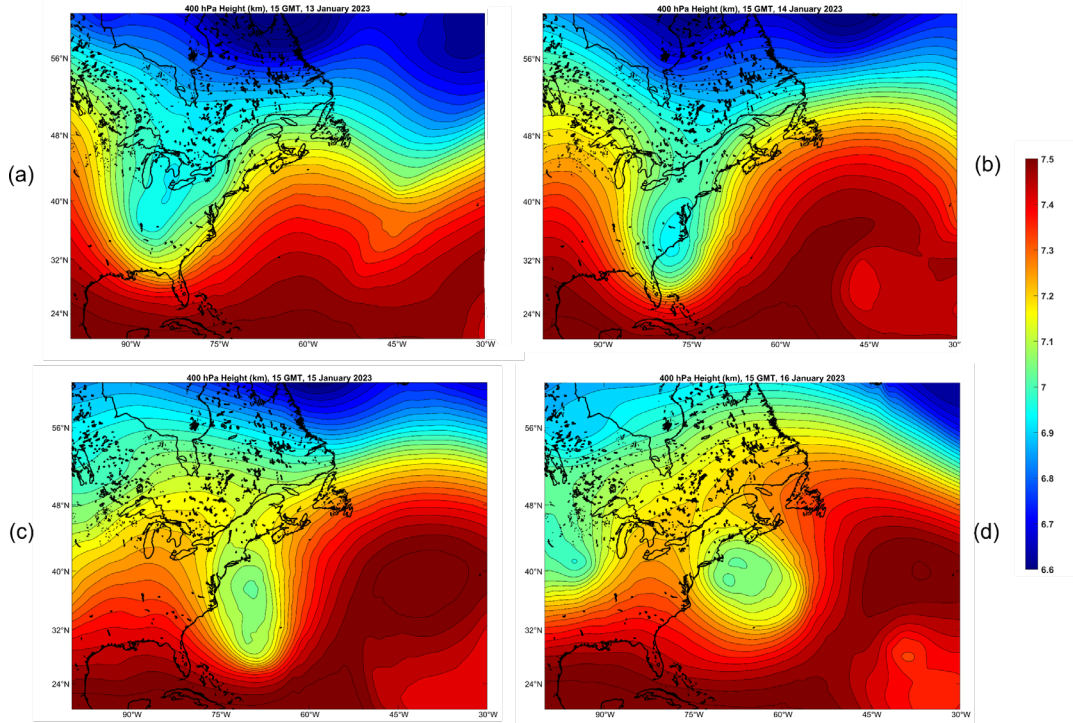


Figure 18: 400 hPa geopotential height (km) at 15:00 GMT on January 13th (a), 14th (b), 15th (c), and 16th (d). From ERA-5 reanalyses.

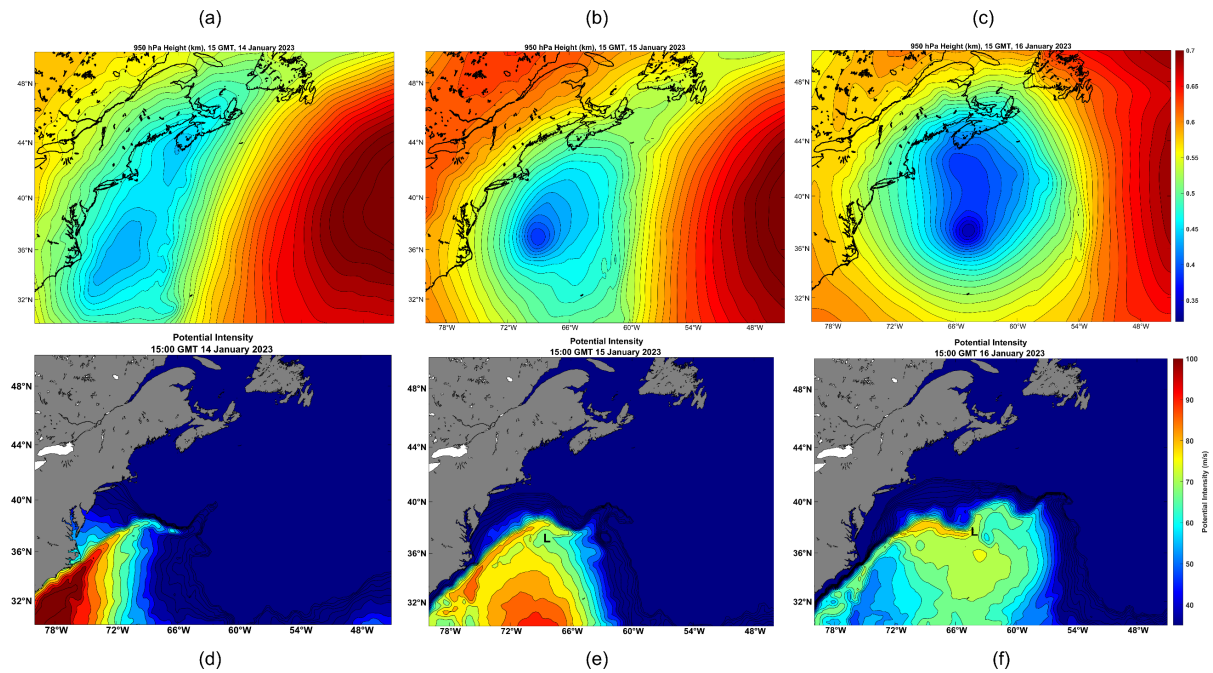


Figure 19: The 950 hPa geopotential height (km) at 15:00 GMT on January 14th (a), 15th (b), 16th (c); the V_{pm} field on January 14th (d), 15th (e), and 16th (f). In (e) and (f) the "L" shows the position of the 950 hPa cyclone center at the time of the chart. From ERA-5 reanalyses.

As the upper tropospheric cyclone begins to pull out toward the northeast on the 16th, the surface cyclone intensifies in the region of large V_{pm} south of the Gulf Stream, while the more gradual warming of the surface air in the region of small V_{pm} north of the Stream yields surface pressure falls, but not as concentrated as in the cyclop to the south.

Although the evolution of the upper tropospheric cyclone differs in detail from the previously examined cases, and the sharp gradient of sea surface temperature across the north wall of the Gulfstream clearly plays a role here, in other respects the development of this subtropical cyclone resembles that of other cyclops, developing in regions of substantial thermodynamic potential that result from cooling aloft on synoptic time and space scales.

f. A Kona Storm

Hawaiians use the term “Kona Storm” to describe cold-season storms that typically form west of Hawaii and often bring damaging winds and heavy rain to the islands. The term “Kona” translates to “leeward”, which in this region means the west side of the islands. They may have been first described in the scientific literature by Daingerfield (1921). Simpson (1952) states that Kona Storms possess “cold-core characteristics, with winds and rainfall amounts increasing with distance from the low-pressure center and reaching a maxima at a radius of 200 to 500 mi. However, with intensification, this cyclone may develop warm-core properties, with rainfall and wind profiles bearing a marked resemblance to those of the tropical cyclone.” In general, Simpson’s descriptions of the later stages of some Kona Storms are consistent with their being cyclops. But it should be noted that the term is routinely applied to cold-season storms that bring hazardous conditions to Hawaii regardless of whether they have developed warm cores. Here we focus on those that do, providing as a single example the Kona Storm of 19 December 2010. A visible satellite image of this storm is shown in Figure 20.

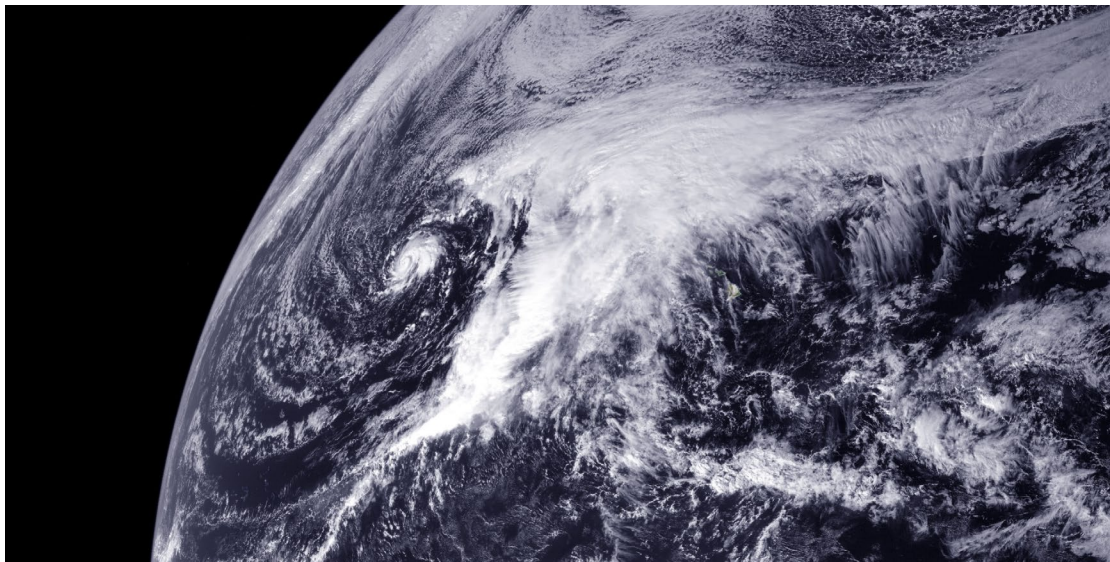


Figure 20: Geostationary satellite visible image showing a Kona Storm at 00 GMT on 19 December 2010. The Kona Storm is the small-scale cyclone left of the major cloud mass.

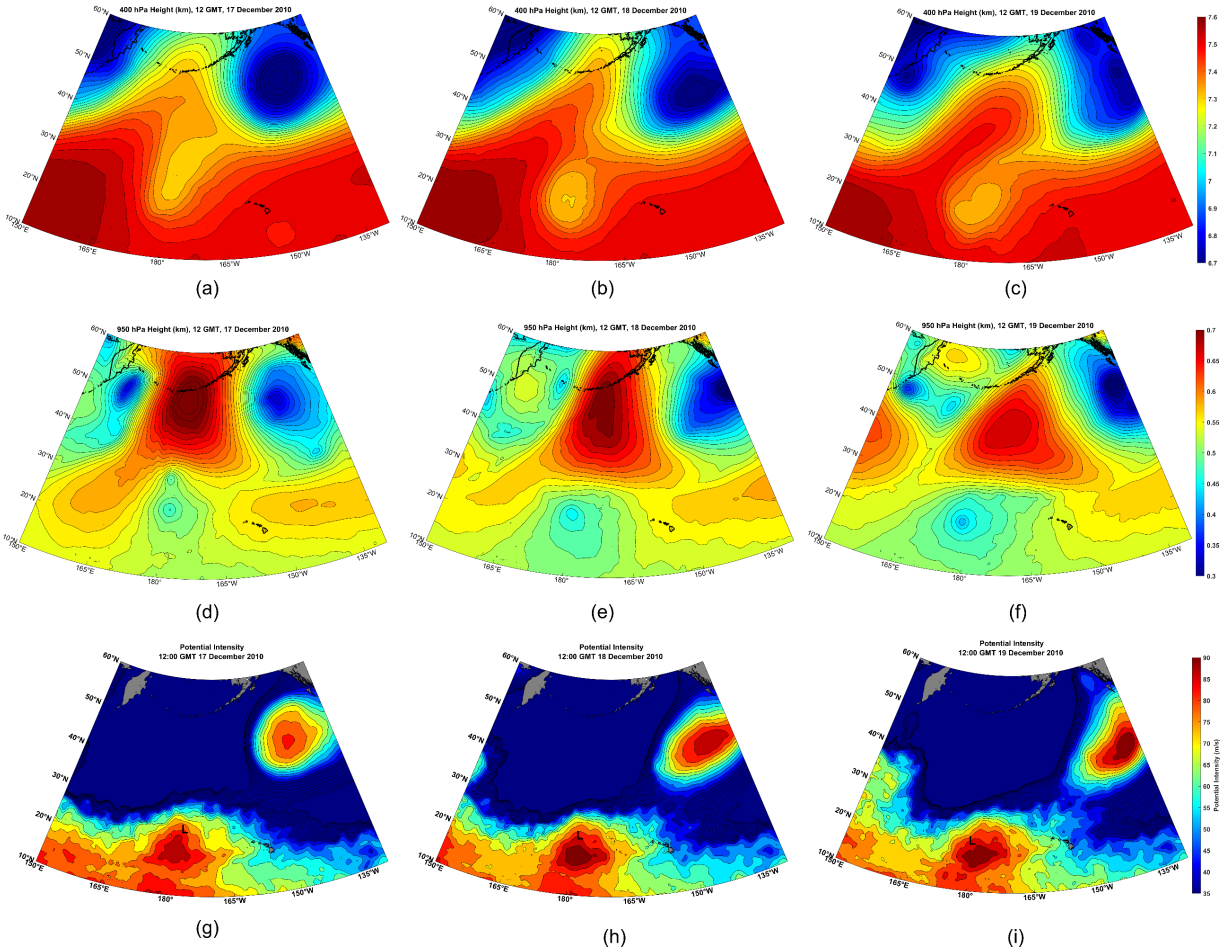


Figure 21: Sequence of 400 hPa geopotential height charts (km; (a)-(c)), 950 hPa geopotential heights (km; (d)-(f)), and V_{pm} ((g)-(i)) at 12:00 GMT on December 17th ((a), (d), (g)), December 18th ((b), (e), (h), and December 19th ((c), (f), (i)) 2010. The “L”s in ((g)-(i)) denote the positions of the 950 hPa cyclone center. From ERA-5 reanalyses.

As with all known cyclops, the December 2010 Kona Storm developed under a cold-core cutoff cyclone aloft, as shown in Figure 21. The upper-level cyclone had a long and illustrious history before December 18th, having meandered over a large swath of the central North Pacific. But beginning on December 17th, the cutoff cyclone made a decisive swing southward over waters with higher values of V_{pm} . A broad surface cyclone was present underneath the cold pool aloft on all three days, but developed a tight inner core on the 19th as the cold pool slowly drifted over a region of higher potential intensity.

This example of a Kona Storm developed in a region of modest climatological potential intensity that was, however, substantially enhanced by the cutoff cyclone aloft. For example, on December 17th, the convective (unmodified) potential intensity at the position of the 950 hPa cyclone center was about 55 ms⁻¹, compared to the 75-80 ms⁻¹ values of the modified potential intensity. One can only speculate whether a surface flux-driven cyclone would have developed without the enhanced cooling associated with the cutoff cyclone aloft.

Figure 22 shows the 950 hPa geopotential height field of another Kona Storm, that of of March, 1951. The storm, at that time, was classified by the Joint Typhoon Warning Center as a tropical cyclone, but the climatological potential intensity there at that time of year could not have supported any tropical cyclone. Figure 22c shows that substantial V_{pm} was associated with a cutoff cyclone in the upper troposphere, making possible the existence of an cyclop.

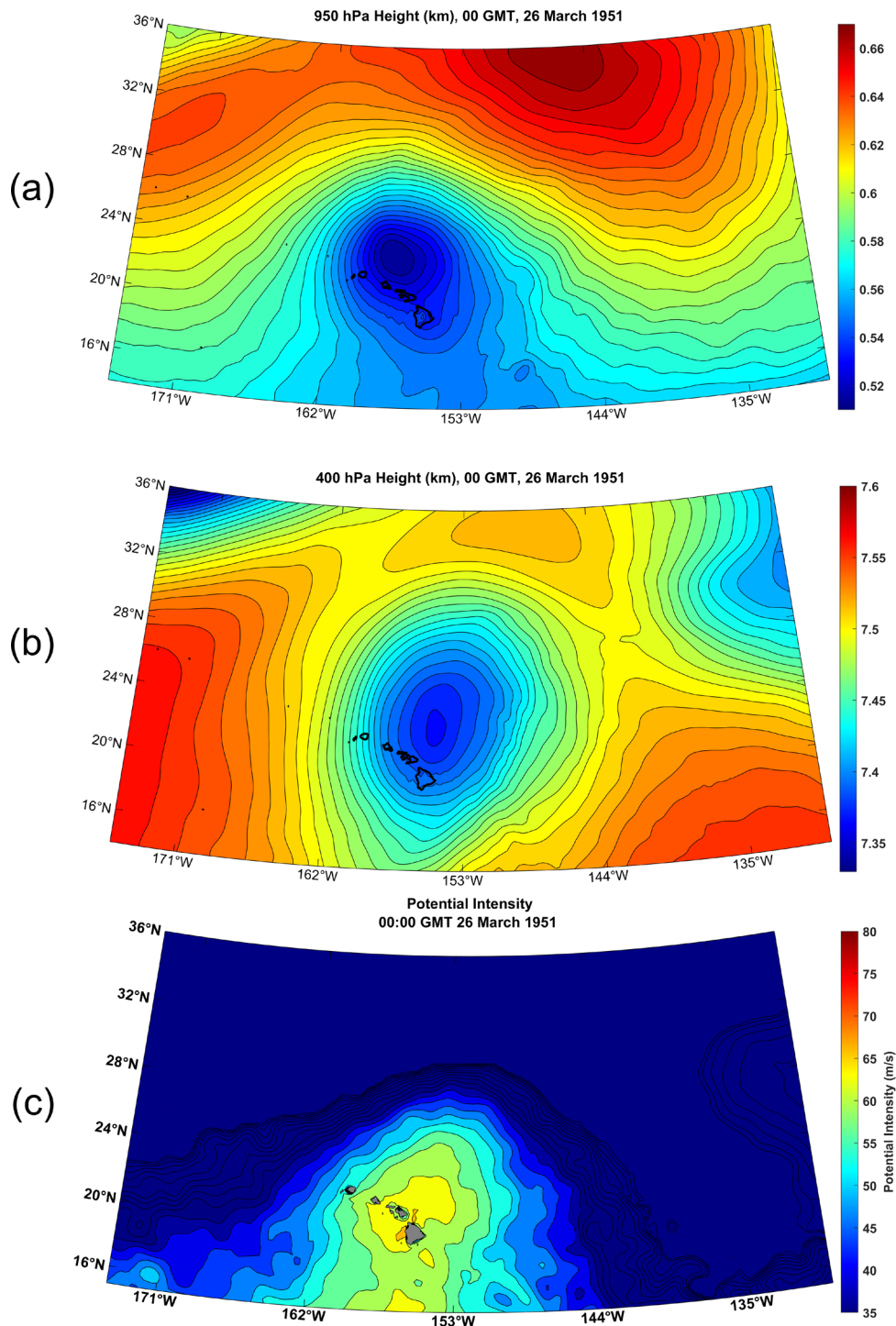


Figure 22: Kona Cyclone of March, 1951. Fields are shown at 00 GMT on 26 March: a): 950 hPa geopotential height (km), b): 400 hPa geopotential height (km), and c): V_{pm} .

4. Variations on the Theme

We here are attempting to distinguish a class of cyclone, cyclops, from other cyclonic storms by their physics, not by the regions in which they develop. Here we present a case of an actual tropical cyclone in the Mediterranean that we do not identify as an cyclop.

a. Cyclone Zorbas

The cyclone known as Zorbas developed just north of Libya on 27 September 2018 and moved northward and then northeastward across the Peloponnese and the Aegean (Figure 23), dissipating in early October. The storm killed several people and did millions of dollars of damage.



Figure 23: Track of Cyclone Zorbas, from 27 September through 2 October, 2018.

The antecedent (actual, not modified) potential intensity distribution, on 26 September, is displayed in Figure 24. In much of the Mediterranean, potential intensity was typical of tropical warm pools with values approaching 80 ms^{-1} . As with most medicanes, Zorbas was triggered by an upper tropospheric Rossby wave breaking event (Figure 25), but in this case the cold pool aloft did little to enhance the potential intensity. Zorbas was therefore a classical case of a tropical cyclone resulting from tropical transition (Bosart and Bartlo 1991; Davis and Bosart 2003, 2004) and would not qualify as an cyclop. Note that while the approach of the upper-level cyclone did not appreciably alter the potential intensity, it almost certainly humidified the middle troposphere, making genesis somewhat more likely.

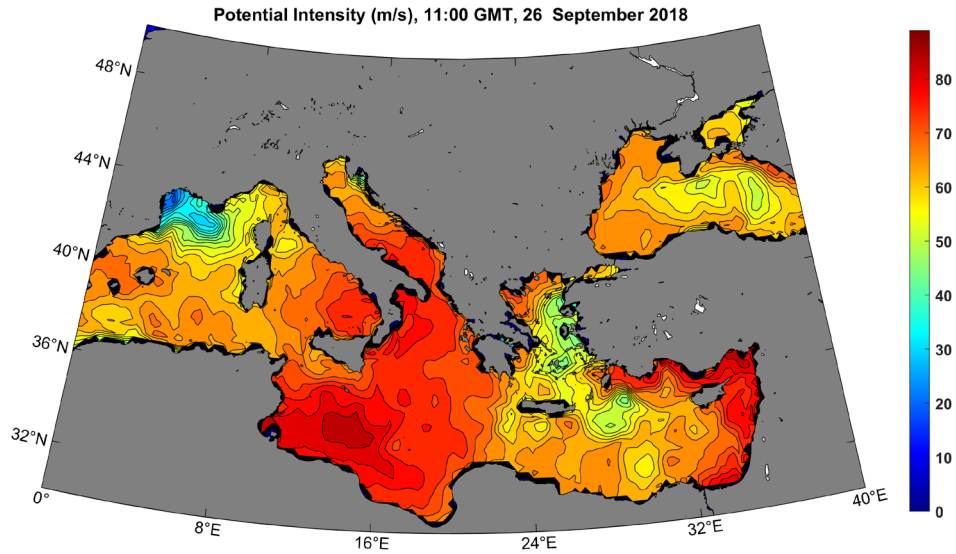


Figure 24: Potential intensity distribution in the Mediterranean and Black Seas, 11 GMT on 26 September 2018.

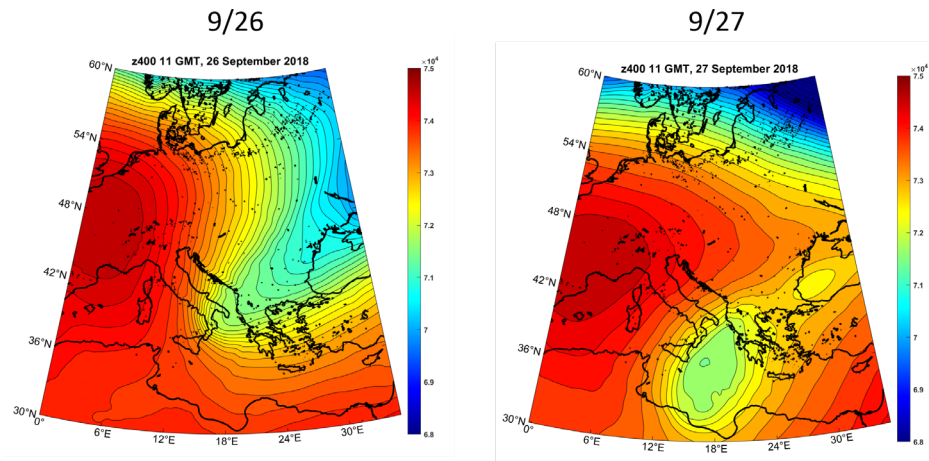


Figure 25: 400 hPa geopotential height (km) at 11 GMT on 26 September (left) and 27 September (right), 2018, from ERA-5 reanalyses.

b. Cyclone Daniel

Cyclone Daniel of 2023 was the deadliest Mediterranean surface flux-driven cyclone in recorded history, with a death toll exceeding 11,000, most of whom perished in floods owing to the catastrophic failure of two dams near Derna, Libya. This flooding was the worst in the recorded history of the African continent. Figure 26 shows the track of Daniel's center and a visible satellite image of the storm as it approached landfall in Libya in shown in Figure 27. Daniel became a surface flux-driven cyclone off the west coast of the Peloponnese on September 5th, made landfall near Benghazi, Libya, on September 10th and dissipated over Egypt on the 12th.



Figure 26: Track of Storm Daniel at 6-hour intervals, beginning September 5th and ending September 12th, 2023.

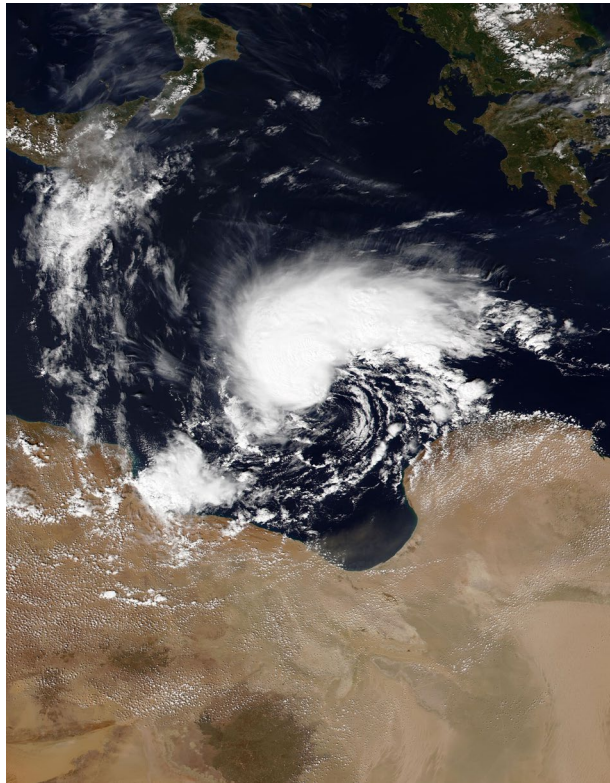


Figure 27: NOAA-20 VIIRS image of Storm Daniel at 12 GMT 9 September 2023, as it approached the Libyan coast.

As with Zorbas, the antecedent potential intensity was high throughout the Mediterranean south and east of Italy and Sicily, and the event was triggered by a Rossby wave breaking event (Figure 27). And as with Zorbas, the cutoff cyclone aloft was not strong enough to have much effect on the potential intensity but acted as a trigger for the tropical cyclone that Daniel became. This was another classic case of tropical transition, and not a cyclop.

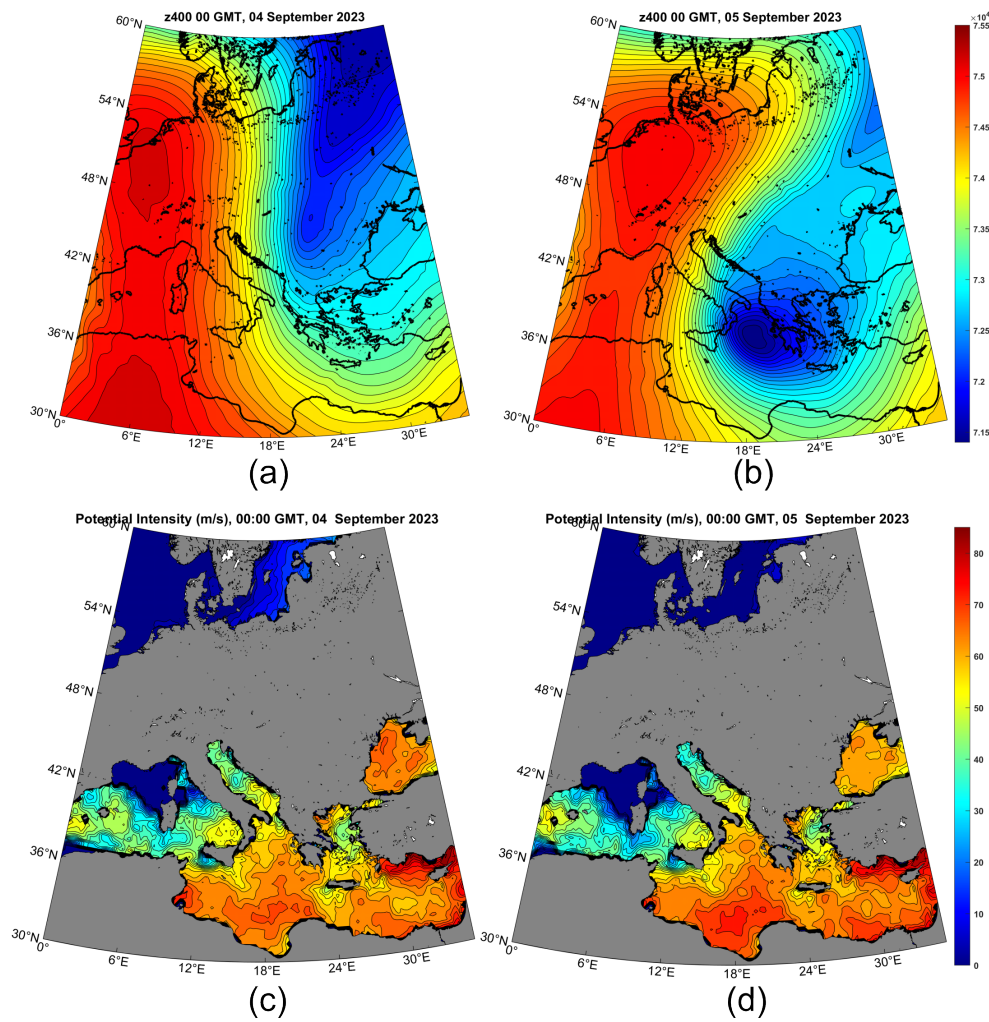


Figure 28: 400 hPa geopotential height (km; (a)-(b)) and actual potential intensity (ms^{-1} ; (c)-(d)) at 00 GMT September 4th ((a) and (c)) and 5th ((b) and (d)), from ERA-5 reanalyses.

Yet Storm Daniel differed from Zorbas in one important respect: As it approached the Libyan coast around September 10th, it came under the influence of strong high-level potential vorticity (PV) advection owing to a mesoscale “satellite” PV mass rotating around the principal upper-level cutoff cyclone (Figure 29). The quasi-balanced forcing associated with the superposition of the high-level PV anomaly with the surface-based warm core probably contributed to Daniel’s intensification which, remarkably for a surface flux-driven cyclone, continued after landfall (Hewson et al. 2024).

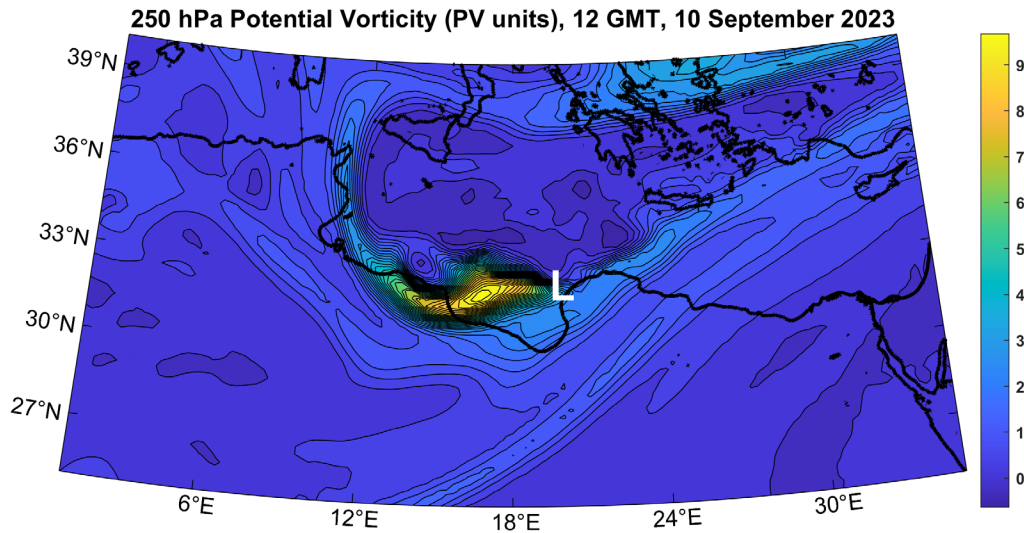


Figure 29: Potential vorticity (PV units, $10^{-6} \text{ K kg}^{-1} \text{ m}^2 \text{ s}^{-1}$) at 250 hPa at 12 GMT on 10 September, 2023. The white “L” marks the approximate surface center of Daniel at this time.

5. Summary

We here argue that many of the cyclonic storms called medicanes, polar lows, subtropical cyclones, and Kona storms operate on the same physics and ought to be identified as a single class of storms that we propose to call cyclops. Like classical tropical cyclones, these are driven primarily by wind-dependent surface enthalpy (latent and sensible heat) fluxes, but unlike classical TCs, there is little or no climatological potential intensity for the storms. Rather, the development and approach of strong, cold-core cyclones in the upper troposphere cools and moistens the column through dynamical lifting, giving rise to mesoscale to synoptic scale columns with elevated potential intensity and humidity, and reduced wind shear – ideal embryos for the development of surface flux-driven cyclones.

We do not expect cyclops to last as long as classical TCs. In the first place, the conditions that enable such storms are confined in space and transient in time. For example, the cutoff cyclone aloft is often re-absorbed into the main baroclinic flow. In addition, the strong surface enthalpy fluxes that power cyclop also increase the enthalpy of the otherwise spatially limited cold columns in which they form, reducing over time the thermodynamic disequilibrium between the air column and the sea surface. A back-of-the-envelope estimate for the time to destroy the initial thermodynamic disequilibrium is on the order of days. By contrast, even the strongest classical TCs do not sufficiently warm the large expanses of the tropical troposphere they influence to appreciably diminish the large-scale potential intensity of tropical warm pools.

Not all cyclonic storms that have been called polar lows, medicanes, subtropical cyclones, or Kona storms meet our definition of cyclop. The literature is full of papers on polar lows that have

been traced to something more nearly like classical baroclinic instability acting in an airmass of anomalously low static stability (e.g. Sardie and Warner 1985). Many storms identified as Kona storms because of their location and season, and which developed under cold cyclones aloft, never received much of a boost from surface fluxes and therefore would not be classified as cyclops. And, as we described in the last section, two strong Mediterranean cyclones, Zorbas of 2018 and Daniel of 2023, developed in environments of plenty of climatological potential intensity and formed via the tropical transition process.

Clearly, there exists a continuum between pure tropical transition, in which synoptic-scale dynamics play no role in setting up the potential intensity, and pure cyclops in which synoptic-scale processes create all the potential intensity that drives the storm. We might think of a triangular phase space in which the vertices are pure baroclinic cyclones, pure tropical cyclones, and cyclops, with real storms migrating through that phase space over time, as in phase-space diagrams of Hart (2003).

Synoptic scale processes, like Rossby wave breaking, are essential not only for triggering cyclops but for providing conducive thermodynamic and kinematic environments for their development. As such, forecasters must account for both the triggering potential and mesoscale to synoptic scale environmental development in predicting the formation and evolution of cyclops. The modified potential intensity (V_{pm}) introduced here may prove to be valuable diagnostic and can easily be calculated from NWP model output. To simulate cyclops, NWP models need to make accurate forecasts of baroclinic processes that lead to the formation and humidification of deep cold pools aloft, and be able to handle surface fluxes and other boundary layer processes essential to the formation of surface flux-driven cyclones. And, as with tropical cyclones, coupling to the ocean is essential for accurate intensity prediction.

Finally, we hope that researchers will focus on the essential physics of cyclops regardless of where in the world they occur. Casting a broader geographical net will harvest a greater sample of such storms and should lead to more rapid progress in understanding and forecasting them.

Appendix

Potential intensity is a measure of the maximum surface wind speed that can be achieved by a cyclone fueled entirely by surface enthalpy fluxes. It is defined (see Rousseau-Rizzi and Emanuel (2019) for an up-to-date definition):

$$V_p^2 = \frac{C_k}{C_D} \frac{T_s - T_o}{T_o} (h_0^* - h_b), \quad (\text{A1})$$

Where C_k and C_D are the surface exchange coefficients for enthalpy and momentum, T_s and T_o are the absolute temperatures of the surface and outflow layer, h_0^* is the saturation moist static energy of the sea surface, and h_b is the moist static energy of the boundary layer.

Using the relation $T\delta s = \delta h$, where s is moist entropy, we can re-write (A1) slightly as

$$V_p^2 = \frac{C_k}{C_D} \frac{T_s - T_o}{T_o} T_s (s_0^* - s_b). \quad (\text{A2})$$

Next, we assume that the troposphere near cyclops has a nearly moist adiabatic lapse rate, and the moist entropy of the boundary layer is equal to the saturation moist entropy, s^* , of the troposphere; i.e., that the troposphere is neutrally stable to moist adiabatic ascent from the boundary layer. Under these conditions, (A2) may be re-written

$$V_p^2 = \frac{C_k}{C_D} \frac{T_s - T_o}{T_o} T_s (s_0^* - s^*). \quad (\text{A3})$$

Here s^* is constant with altitude, since the troposphere is assumed to have a moist adiabatic lapse rate.

Referring to Figure 1a in the main text, we want to know what the potential intensity is under the cutoff cyclone aloft *before* the atmosphere underneath it has started to warm up under the influence of surface enthalpy fluxes. But in reality, this warming commences as soon as the system moves over relatively warm water. We can infer what the temperature, or s^* , is under the cutoff cyclone by relating the temperature perturbation under the cyclone to the geopotential perturbation associated with the cutoff low.

We begin with the perturbation hydrostatic equation in pressure coordinates:

$$\frac{\partial \phi'}{\partial p} = -\alpha', \quad (\text{A4})$$

where ϕ' is the perturbation geopotential and α' is the perturbation specific volume. Since the latter is a function of pressure and s^* only, we can use the chain rule and one of the Maxwell relations from thermodynamics to write (A4) as

$$\frac{\partial \phi'}{\partial p} = - \left(\frac{\partial T}{\partial p} \right)_{s^*} s^{*'} . \quad (\text{A5})$$

Now, since $s^{*'}$ does not vary with altitude, we can integrate (A5) from the surface to the local tropopause to yield

$$\phi_{cl}' - \phi_s' = (T_s - T_o) s^{*'}. \quad (\text{A6})$$

where ϕ_{cl}' is the geopotential perturbation associated with the cutoff cyclone aloft and ϕ_s' is the near-surface geopotential perturbation.

We want to know how cold the air is under the cutoff low *before* the surface pressure has dropped, so we can use (A6) to find the temperature (s^*) perturbation that would be found under the cutoff cyclone in the absence of a surface pressure perturbation:

$$s^{*'} = \frac{\phi_{cl}'}{T_s - T_o}. \quad (A7)$$

Using this, the modified definition of potential intensity, V_{pm} , can be written from (A1) as

$$V_{pm}^2 = \frac{C_k}{C_D} \frac{T_s - T_o}{T_o} T_s \left(s_0^* - s_e^* - \frac{\phi_{cl}'}{T_s - T_o} \right), \quad (A8)$$

or equivalently,

$$V_{pm}^2 = V_p^2 - \frac{C_k}{C_D} \frac{T_s}{T_o} \phi_{cl}', \quad (A9)$$

where V_p is the unperturbed potential intensity.

For the purposes of the present work, we defined the perturbation as the difference between the actual geopotential and its climatological value determined from monthly mean values over the period 1979–2023, and we estimate the cutoff cyclone geopotential perturbation at 400 hPa.

References

- Bosart, L. F., and J. A. Bartlo, 1991: Tropical storm formation in a baroclinic environment. *Mon Wea Rev*, **119**, 1979–2013.
- Cangliosi, J. P., P. Papin, and J. L. Beven, 2023: *Unnamed tropical storm (AL012023)*. https://www.nhc.noaa.gov/data/tcr/AL012023_Unnamed.pdf.
- Cavicchia, L., H. von Storch, and S. Gualdi, 2014: A long-term climatology of medicanes. *Clim. Dyn.*, **43**, 1183–1195, <https://doi.org/10.1007/s00382-013-1893-7>.
- Chavas, D. R., and K. A. Emanuel, 2014: Equilibrium tropical cyclone size in an idealized state of axisymmetric radiative–convective equilibrium. *J Atmos Sci*, **71**, 1663–1680.
- Cronin, T. W., and D. R. Chavas, 2019: Dry and Semidry Tropical Cyclones. *J. Atmospheric Sci.*, **76**, 2193–2212, <https://doi.org/10.1175/jas-d-18-0357.1>.

- Daingerfield, L. H., 1921: KONA STORMS. *Mon. Weather Rev.*, **49**, 327–329, [https://doi.org/10.1175/1520-0493\(1921\)49<327:ks>2.0.co;2](https://doi.org/10.1175/1520-0493(1921)49<327:ks>2.0.co;2).
- Davis, C. A., and L. F. Bosart, 2003: Baroclinically induced tropical cyclogenesis. *Mon. Weather Rev.*, **131**, 2730–2747, [https://doi.org/10.1175/1520-0493\(2003\)131<2730:BITC>2.0.CO;2](https://doi.org/10.1175/1520-0493(2003)131<2730:BITC>2.0.CO;2).
- , and ———, 2004: The TT problem: Forecasting the tropical transition of cyclones. *Bull. Am. Meteorol. Soc.*, **85**, 1657–1662, <https://doi.org/10.1175/BAMS-85-11-1657>.
- Emanuel, K., 2005: Genesis and maintenance of “Mediterranean hurricanes.” *Adv Geosci*, **2**, 217–220.
- , 2010: Tropical cyclone activity downscaled from NOAA-CIRES reanalysis, 1908-1958. *J Adv Model Earth Sys*, **2**, 1–12.
- Fita, L., and E. Flaounas, 2018: Medicanes as subtropical cyclones: the December 2005 case from the perspective of surface pressure tendency diagnostics and atmospheric water budget. *Q. J. R. Meteorol. Soc.*, **144**, 1028–1044, <https://doi.org/10.1002/qj.3273>.
- Hart, R. E., 2003: A cyclone phase space derived from thermal wind and thermal asymmetry. *Mon. Weather Rev.*, **131**, 585–616, [https://doi.org/10.1175/1520-0493\(2003\)131<0585:acpsdf>2.0.co;2](https://doi.org/10.1175/1520-0493(2003)131<0585:acpsdf>2.0.co;2).
- Hewson, T., and Coauthors, 2024: Medicane Daniel: an extraordinary cyclone with devastating impacts. *ECMWF Newsl.*, **179**, 33–47.
- McIntyre, M. E., and T. N. Palmer, 1983: Breaking planetary waves in the stratosphere. *Nature*, **305**, 593–600, <https://doi.org/10.1038/305593a0>.
- McTaggart-Cowan, R., G. D. Deane, L. F. Bosart, C. A. Davis, and T. J. Galarneau, 2008: Climatology of tropical cyclogenesis in the North Atlantic (1948–2004). *Mon. Weather Rev.*, **136**, 1284–1304, <https://doi.org/10.1175/2007MWR2245.1>.
- , T. J. Galarneau, L. F. Bosart, R. W. Moore, and O. Martius, 2013: A global climatology of baroclinically influenced tropical cyclogenesis. *Mon. Weather Rev.*, **141**, 1963–1989, <https://doi.org/10.1175/MWR-D-12-00186.1>.
- Miglietta, M. M., D. Carnevale, V. Levizzani, and R. Rotunno, 2021: Role of moist and dry air advection in the development of Mediterranean tropical-like cyclones (medicanes). *Q. J. R. Meteorol. Soc.*, **147**, 876–899, <https://doi.org/10.1002/qj.3951>.
- Nastos, P. T., K. Karavana Papadimou, and I. T. Matsangouras, 2018: Mediterranean tropical-like cyclones: Impacts and composite daily means and anomalies of synoptic patterns. *High Impact Atmospheric Process. Mediterr.*, **208**, 156–166, <https://doi.org/10.1016/j.atmosres.2017.10.023>.

- Nordeng, T. E., and E. A. D.-:10. 1034/j. 1600-0870. 1992. 00001. x Rasmussen, 1992: A most beautiful polar low. A case study of a polar low development in the Bear Island region. *Tellus A*, **44**, 81–99.
- Pytharoulis, I., G. C. Craig, and S. P. Ballard, 1999: Study of the Hurricane-like Mediterranean cyclone of January 1995. *Phys. Chem. Earth Part B Hydrol. Oceans Atmosphere*, **24**, 627–632, [https://doi.org/10.1016/S1464-1909\(99\)00056-8](https://doi.org/10.1016/S1464-1909(99)00056-8).
- Romero, R., and K. D.-:10. 1002/jgrd. 50475 Emanuel, 2013: Medcane risk in a changing climate. *J Geophys Res*, **118**.
- Rotunno, R., and K. A. Emanuel, 1987: An air-sea interaction theory for tropical cyclones. Part II. *J Atmos Sci*, **44**, 542–561.
- Rousseau-Rizzi, R., and K. Emanuel, 2019: An evaluation of hurricane superintensity in axisymmetric numerical models. *J. Atmospheric Sci.*, **76**, 1697–1708, <https://doi.org/10.1175/jas-d-18-0238.1>.
- Sardie, J. M., and T. T. D.-:10. 1111/j. 1600-0870. 1985. tb00444. x Warner, 1985: A numerical study of the development mechanisms of polar lows. *Tellus A*, **37A**, 460–477.
- Simpson, R. H., 1952: Evolution of the Kona storm: A subtropical cyclone. *J. Atmospheric Sci.*, **9**, 24–35, [https://doi.org/10.1175/1520-0469\(1952\)009<0024:EOTKSA>2.0.CO;2](https://doi.org/10.1175/1520-0469(1952)009<0024:EOTKSA>2.0.CO;2).
- Tomita, H., and R. Tanaka, 2024: Ocean surface warming and cooling responses and feedback processes associated with polar lows over the Nordic seas. *J. Geophys. Res. Atmospheres*, **129**, e2023JD040460, <https://doi.org/10.1029/2023JD040460>.
- Tous, M., and R. D.-:10. 1002/joc. 3428 Romero, 2013: Meteorological environments associated with medcane development. *Int. J. Climatol.*, **33**, 1–14.
- Velez-Pardo, M., and T. W. Cronin, 2023: Large-scale circulations and dry tropical cyclones in direct numerical simulations of rotating Rayleigh-Bénard convection. *J. Atmospheric Sci.*, <https://doi.org/10.1175/JAS-D-23-0018.1>.
- Yanase, W. and co-authors, 2016: Climatology of polar lows over the Sea of Japan using the JRA-55 reanalysis. *J Clim.*, **29**, 419–437.
- Yarovaya, D. A., V. V. Efimov, M. V. Shokurov, S. V. Stanichnyi, and V. S. Barabanov, 2008: A quasitropical cyclone over the Black Sea: Observations and numerical simulation. *Phys. Oceanogr.*, **18**, 154–167, <https://doi.org/10.1007/s11110-008-9018-2>.
- Zhang, W., G. Villarini, E. Scoccimarro, and F. Napolitano, 2021: Examining the precipitation associated with medcanes in the high-resolution ERA-5 reanalysis data. *Int. J. Climatol.*, **41**, E126–E132, <https://doi.org/10.1002/joc.6669>.
- Zhang, Y., Z. Meng, F. Zhang, and Y. Weng, 2014: Predictability of tropical cyclone intensity evaluated through 5-yr forecasts with a convection-permitting regional-scale model in the Atlantic basin. *Wea Forecast.*, **29**, 1003–1022.